Mathematical Modelling of a Metal Hydride Hydrogen Storage System

by

Brendan David MacDonald
B.A.Sc., University of Waterloo, 2004

A Thesis Submitted in Partial Fulfillment of the
Requirements for the Degree of

MASTER OF APPLIED SCIENCE

in the Department of Mechanical Engineering

Mathematical Modelling of a Metal Hydride Hydrogen Storage System

by

Brendan David MacDonald
B.A.Sc., University of Waterloo, 2004

Supervisory Committee

Dr. Andrew Rowe (Dept. of Mechanical Engineering)

Supervisor

Dr. Brad Buckham (Dept. of Mechanical Engineering)

Departmental Member

Dr. Zuomin Dong (Dept. of Mechanical Engineering)

Departmental Member

Supervisory Committee

Dr. Andrew Rowe (Dept. of Mechanical Engineering)
Supervisor

Dr. Brad Buckham (Dept. of Mechanical Engineering)
Departmental Member

Dr. Zuomin Dong (Dept. of Mechanical Engineering)
Departmental Member

Abstract

In order for metal hydride hydrogen storage systems to compete with existing energy storage technology, such as gasoline tanks and batteries, it is important to have fast reaction rates, especially quick refill times. Improving the hydriding rate involves enhancing the heat transfer within the reaction bed. To complement experimental investigations, a two-dimensional transient model has been developed to describe the heat and mass transfer phenomena within a metal hydride bed. The metal hydride model is thermally coupled to a fuel cell through heat transfer relations and utilized to compare different heat transfer enhancements and storage tank configurations. Three cases are simulated: a base case with no heat transfer enhancements, a case with fins attached to the outside of the tank, and a case with an annular tank design. The results demonstrate that the annular metal hydride tank meets the requirements of the fuel cell while providing a robust and compact hydrogen storage system.

Table of Contents

List of Figures

List of Tables

Nomenclature

A_f	surface area of each fin (m^2)
A_o	area of the interior tube opening (m^2)
A_{side}	surface area of the side of the tank (m^2)
A_t	total surface area of the tank (m^2)
c_{pa}	specific heat of the air ($J\ kg^{-1}K^{-1}$)
c_{pg}	specific heat of the hydrogen gas ($J\ kg^{-1}K^{-1}$)
c_{ps}	specific heat of the metal hydride alloy ($J\ kg^{-1}K^{-1}$)
C_a	absorption constant
C_d	desorption constant
D	diameter of the tank (m)
D_o	diameter of the interior tube opening (m)
E_a	absorption activation energy ($J\ mol^{-1}$)
E_d	desorption activation energy ($J\ mol^{-1}$)
f	friction factor
g	acceleration due to gravity ($m\ s^{-2}$)
h	heat transfer coefficient ($W\ m^{-2}K^{-1}$)
h_{base}	heat transfer coefficient for the base case ($W\ m^{-2}K^{-1}$)
h_{fin}	effective heat transfer coefficient for the finned wall ($W\ m^{-2}K^{-1}$)
h_n	heat transfer coefficient during the off-cycle ($W\ m^{-2}K^{-1}$)
h_{si}	heat transfer coefficient in the interior tube ($W\ m^{-2}K^{-1}$)
h_{side}	heat transfer coefficient over the side wall ($W\ m^{-2}K^{-1}$)
H	hydrogen atoms
k	thermal conductivity ($W\ m^{-1}K^{-1}$)
k_{Al}	thermal conductivity of the aluminum wall ($W\ m^{-1}K^{-1}$)
k_e	effective thermal conductivity of the metal hydride bed ($W\ m^{-1}K^{-1}$)
K	permeability (m^2)
L	length (m)
m	rate of hydrogen absorption ($kg\ m^{-3}s^{-1}$)
m_a	mass flow rate of air ($kg\ s^{-1}$)

m_{abs}	rate of hydrogen absorption (kg $m^{-3}s^{-1}$)
m_{des}	rate of hydrogen desorption (kg $m^{-3}s^{-1}$)
M	metal molecules in a metal hydride alloy
M_g	molecular weight of hydrogen gas (kg $kmol^{-1}$)
N	number of fins
Nu_∞	Nusselt number for fully developed flow
Nu_D	Nusselt number
Nu_m	mean Nusselt number for the entry region
P	perimeter (m)
P_{eq}	equilibrium pressure (kPa)
P_{eqa}	absorption equilibrium pressure (kPa)
P_{eqd}	desorption equilibrium pressure (kPa)
P_g	pressure of the hydrogen gas within the tank (kPa)
Pr	Prandtl number
q	rate of heat transfer (W)
r	radius (m)
r_1	interior radius (m)
r_2	exterior radius (m)
R_g	universal gas constant (J mol^{-1} K^{-1})
R_{fin}	effective thermal resistance due to external fins (K W^{-1})
$R_{t,cond}$	thermal resistance due to conduction (K W^{-1})
$R_{t,conv}$	thermal resistance due to convection (K W^{-1})
$R_{t,mh}$	thermal resistance due to the metal hydride bed (K W^{-1})
$R_{t,tot}$	total thermal resistance (K W^{-1})
Ra_D	Rayleigh number
Re_D	Reynolds number
t	time (s)
th	thickness of a fin (m)
T	temperature inside the metal hydride tank (K)
T_∞	ambient air temperature (K)
T_0	initial temperature of air at start of on-cycle (K)

T_a	air temperature as it exits the stack (K)
T_{air}	average air temperature (K)
T_f	film temperature (K)
T_{in}	air temperature prior to encountering the tank (K)
T_{mh}	temperature of the metal hydride bed (K)
T_{out}	air temperature after encountering the tank (K)
T_s	surface temperature of the metal hydride tank (K)
T_{si}	local temperature of the interior tube wall (K)
T_{side}	temperature of the side of the tank (K)
T_{ss}	steady-state temperature (K)
$T_{w,i}$	interior wall temperature (K)
v_m	mean velocity of the air stream (m s^{-1})
V_g	velocity of the hydrogen gas (m s^{-1})
z	height (m)

Greek Letters

α	thermal diffusivity (m^2 s^{-1})
ΔH	enthalpy change of hydriding reaction (J kg^{-1})
ΔS	entropy change of hydriding reaction (J kg^{-1} K^{-1})
ε	porosity of the metal hydride bed
η_f	fin efficiency
μ_a	dynamic viscosity of the air (Ns m^{-2})
μ_g	dynamic viscosity of the hydrogen gas (Ns m^{-2})
ν	kinematic viscosity (m^2 s^{-1})
ρ_a	density of the air (kg m^{-3})
ρ_{emp}	density of the metal hydride alloy prior to absorbing hydrogen (kg m^{-3})
ρ_g	density of the hydrogen gas (kg m^{-3})
ρ_s	density of the metal hydride bed (kg m^{-3})
ρ_{sat}	saturated density of the metal hydride alloy (kg m^{-3})
τ_{on}	thermal time constant for the on-cycle (s)
τ_{off}	thermal time constant for the off-cycle (s)

Acknowledgements

I would like to thank my supervisor, Dr. Andrew Rowe, for his support. The ways in which this support manifested itself are too numerous to list, but I would like to highlight a few. Andrew's enthusiasm and determination have allowed my own passion for research to flourish, and enabled me to accomplish things I would have previously thought to be inaccessible. His patience and knowledge are quite vast, and these qualities helped my research to take place at a quick pace. Discussions we regularly had regarding how certain research aspects fit into the "big picture" made the research very meaningful and enjoyable. Andrew's exceptional abilities as a supervisor and his faith in me have played a large role in my decision to stay at the University of Victoria for my doctorate work.

A very big thanks to my wonderful wife Sukman MacDonald. Her bottomless well of patience has allowed me to pursue my dreams, and for that I am immensely grateful. Her encouragement has also allowed me to push forward when barriers were encountered.

I would also like to thank my parents, Brian and Kathleen MacDonald, my brother Colin MacDonald, and my good friend, Michael Evans. They were never more than a phone call away, and their support was invaluable, especially my parents, who were available to talk at all hours of the day and night.

I would like to thank Jordan Roszmann for providing the three-dimensional drawings of the fuel cell and the duct work, and Alvin Bergen and Tom Schmeister for assisting with the testing of the Nexa™ fuel cell module.

1 Introduction

1.1 Background

Recently there has been global concern over the increasing concentration of greenhouse gases in the atmosphere, and their contribution to the global warming phenomenon. The Kyoto agreement was created in December 1997 to tackle this issue. Since then, many organizations have been investigating ways of reducing greenhouse gas emissions, dominated by carbon dioxide, by reducing or finding alternatives to fossil fuels. One of the most promising alternatives is the use of hydrogen fuel within a fuel cell. The emissions from a hydrogen fuelled process do not contain carbon dioxide, and in fact contain only water. Therefore, hydrogen has great potential in offering a new "energy currency" and replacing fossil fuels such as refined oil. However, because hydrogen is in gaseous form at room temperature, it is more difficult to store than gasoline, which is in liquid form. Therefore, hydrogen storage is an active area of research. Suitable hydrogen storage methods must be developed before a "hydrogen economy" can be realized.

There are three established methods for storing hydrogen fuel and each of these methods has advantages and disadvantages. The first method is to compress the hydrogen gas and store it in a high-pressure cylinder. The Honda FCX vehicle currently uses a three layer, aluminum - carbon fibre - glass fibre, tank that is capable of storing hydrogen at pressures up to 350 atm (~35,000 kPa) [1]. Another method is to cryogenically liquefy the hydrogen, and store it in liquid form in a dewar. At 1 atm (~100 kPa) the condensation point of hydrogen is approximately 20 K (~-253°C) [2]. The third method is to store the hydrogen in a solid form by allowing it to be absorbed into a metal alloy. Many metals and alloys are capable of reversibly absorbing hydrogen, and once the hydrogen is absorbed the metal or alloy is referred to as a *metal hydride*. The advantages for compressed gaseous storage are the possibility of transporting the gas through hydrogen pipelines, and also the lower mass of the system since only hydrogen and the high-pressure storage vessels are required. Disadvantages are the safety risk of high-pressure vessels, and the energy required to compress the gas. Honda is currently developing a high-pressure storage tank (350 atm) where a newly developed hydrogen absorption material is introduced in the tank to double capacity without increasing the pressure [3]. A possible niche for compressed hydrogen is storage on fuel cell automobiles. Cryogenic liquid hydrogen benefits from the increased density of liquid hydrogen (~70.8 kg m^{-3} [2]) so that less volume is required versus compressed gaseous storage. Disadvantages to liquid storage are the possible heat losses and venting of hydrogen, and the high energy costs associated with liquefaction. Possible niches for liquid hydrogen are transporting hydrogen fuel by tanker truck, and also as bulk storage of hydrogen at local refuelling stations. Metal hydride storage systems can offer improved volumetric capacity to that of liquid storage, utilize low grade energy, allow for tank interchange (not just refuelling), and also provide a safer low pressure package. Disadvantages to metal hydride storage are the increased mass of the system due to the additional weight of the metal alloy, and raw material cost of the alloys can be high depending on which materials are used. Possible niches for metal hydride storage are storage on small-scale vehicles and electronic devices where size is an important design parameter, and also for bulk storage of hydrogen in stationary applications.

1.2 Metal Hydrides

A *reversible metal hydride* is a metallic compound that is capable of absorbing and desorbing hydrogen under varying circumstances. The chemical reaction associated with absorption and desorption is as follows:

$$M+\frac{x}{2}H_2 \leftrightarrow MH_x + heat \qquad (1.1)$$

The *heat* term on the right-hand side of Eq. (1.1) indicates that the forward reaction (absorption) is exothermic, and the backward reaction (desorption) is endothermic. When used for hydrogen storage purposes, the metal alloy is ground into a powder and placed into a tank, usually a cylindrical pressure vessel. Prior to being used for reversible storage of hydrogen the alloy must undergo *activation*, which can involve high temperatures and pressures depending on the alloy. This procedure brings the alloy up to maximum hydrogen capacity and absorption/desorption kinetics [4]. Metal hydrides can be used for many different applications including hydrogen storage, compression, hydrogen separation, or as heat pumps and refrigerators. For the purposes of this thesis the focus will be on metal hydrides used for hydrogen storage.

The thermodynamic behaviour of metal hydride formation is best illustrated by an isothermal pressure-composition (P-C) hysteresis loop, shown in generalized form in Figure 1.1 [4]. Figure 1.1 is labelled to illustrate the mathematical definitions of *hysteresis*, *plateau slope*, and *hydrogen capacity*. The upper curve, with arrows pointing up and to the right, is the absorption curve, and the lower curve, with arrows pointing down and to the left, is the desorption curve. The curves represent the equilibrium pressures (y-axis values) associated with the absorption or desorption reaction for varying hydrogen concentration values (x-axis values) at a fixed temperature.

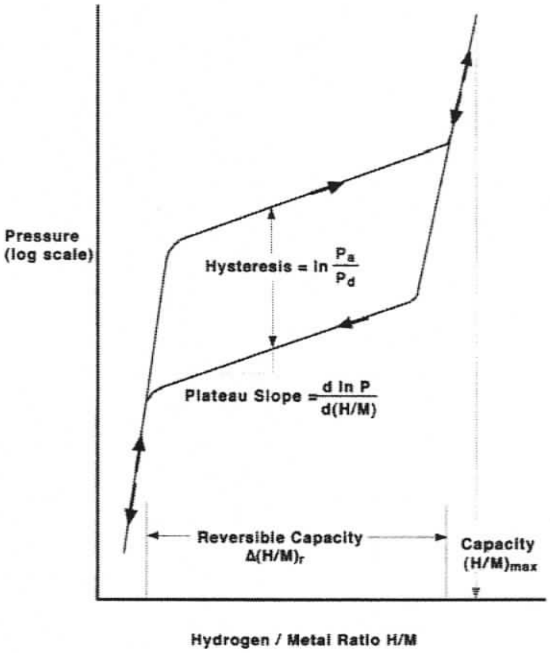

Figure 1.1 – Schematic isothermal pressure-composition hysteresis loop. [4]

If the absorption curve in Figure 1.1 is followed from left to right, this represents the metal hydride alloy absorbing hydrogen. The flat section of the curves is referred to as the *plateau* and this region represents the *reversible* range of hydrogen capacity. The term reversible is used because along this portion of the curve large amounts of hydrogen can be absorbed and desorbed with only small changes in pressure. Beyond the plateau section it is possible to absorb and desorb hydrogen, however the large pressure changes make it inconvenient to do so for practical storage applications. For this same reason it is desirable to use alloys that have a flat plateau slope, so that the pressure variation during filling and emptying can be kept to a minimum. *Hysteresis* refers to the difference in equilibrium pressures between the absorption and desorption reactions. It is desirable to keep hysteresis to a minimum because it results in an energy loss for the system. This energy loss stems from the fact that the tank is filled at a high pressure, yet when emptied at the same temperature provides hydrogen gas at a lower pressure. Another definition provided from Figure 1.1 is the *capacity* of a metal hydride alloy. The *maximum capacity* shown in Figure 1.1 refers to the amount of hydrogen that an alloy can physically absorb, if the hydrogen gas was available at unlimited pressures. The *reversible capacity* refers to the width of the plateau section, since this is the hydrogen storage capacity of the metal hydride alloy under practical operating pressures. Typically, the reversible capacity is noted when listing the capacity of metal hydride alloys. Capacity can be listed in either atomic H/M ratio or weight percent. In calculating weight percent, both H and M are included in the denominator, not only M. [4]

The P-C hysteresis loop is useful for defining some properties of metal hydrides, however in practice it is rare for single temperature values to be used. Thermodynamics dictates that the plateau pressures must increase with temperature, usually close enough to the van't Hoff equation for engineering purposes [4]:

$$\ln P_{eq} = \frac{\Delta H}{RT} - \frac{\Delta S}{R} \tag{1.2}$$

where P is the equilibrium pressure, ΔH and ΔS are the enthalpy and entropy changes of the hydriding reaction, T is the absolute temperature, and R is the gas constant. The isotherms on a P-C plot such as Figure 1.1 tend to follow the same shape when different temperature values are used for a single alloy, but higher temperatures yield higher pressures and lower temperatures yield lower pressures. Since equilibrium pressure is a function of temperature, often temperature is varied to control the absorption and desorption reactions and the input and output pressures. It is normally easier to control temperature to yield a desired pressure, however pressure could also be varied to yield a desired tank temperature.

1.3 Metal Hydride Materials

Hydrogen is a reactive element that has been shown to form hydrides with many metals and alloys. In this section the conventional metal hydride alloy families will be summarized to facilitate understanding of the alloy choices made later in this thesis. In these alloys the hydrogen (H) is usually bonded in interstitial sites in a metallic state with minor distortions of the generally stable H-free alloy structures. To optimize the performance of reversible hydrides, the material scientists have combined strong hydride forming elements (referred to as A) with weak hydriding elements (referred to as B) to form alloys (particularly intermetallic compounds) that have the desired intermediate thermodynamic affinities for hydrogen. The ability to 'interpolate' between the extremes of elemental hydriding behaviour has led to the contemporary reversible hydrides. [4] The conventional metal hydride alloy families to be described here are the AB_5, AB_2, and AB intermetallic compounds.

1.3.1 AB_5 Intermetallic Compounds

The AB_5 family has an extraordinary versatility because many different elemental species can be substituted (at least partially) into the A and B lattice sites. The A-elements tend to be one or more of the lanthanides (atomic numbers 57-71). The B-elements are based on Ni with many other possible substitutional elements such as Co, Al, Mn, Fe, Cu, Sn, Si, Ti, etc. Modern commercial AB_5 hydriding alloys are mostly based on the use of the lanthanide mixture mischmetal (Mm = Ce + La + Nd + Pr) for the A-side and Ni + Al +

Mn + Co + … on the B-side. [4] It should be noted that the alloys in this and the other conventional alloy families can be tuned by altering the composition of the alloy to meet the specific needs of the hydrogen storage application, typically the desired output pressure at certain temperature ranges.

The AB_5 family has a broad range of PCT (Pressure-Composition-Temperature) versatility and tunability, with the 25°C plateau pressure varying over at least three orders of magnitude depending on the composition. Hysteresis is usually quite low for the AB_5s, and it is possible to attain rather flat plateaus even with multicomponent alloys. H-capacity is on the low side, not exceeding 1.3 wt.% on the reversible capacity basis. Alloy raw material cost is slightly high, at least in comparison to the other families (AB_2 and AB). The AB_5 alloys also have good tolerance to small amounts of O_2 and H_2O impurities in the hydrogen stream. [4]

1.3.2 AB_2 Intermetallic Compounds

Like the AB_5s, the AB_2 family represents a large and versatile group of hydriding materials with PCT values of interest for the ambient temperature range. The A-elements are often from the IVA group (Ti, Zr, Hf) and/or rare earth series (atomic numbers 57-71) or Th. The B-elements can be a variety of transition or non-transition metals with a preference towards the atomic numbers 23-26 (V, Cr, Mn, Fe). A wide variety of substitutions are possible for both A- and B-elements, thus providing a high degree of fine tuning of PCT properties. [4]

The PCT properties of AB_2 alloys can be adjusted over ranges of temperature and pressure that cover the 1-10 atm (~100-1000 kPa), 0-100°C range (the range that is typically of use for most storage applications). The H-capacities of AB_2 alloys are comparable to AB_5s on a reversible capacity basis but generally higher on a maximum capacity basis. The AB_2s often suffer from a less distinct, narrower plateau than AB_5s. When larger temperature and pressure ranges are available from the storage application, AB_2s tend to show higher capacities than AB_5s. The AB_2 alloys offer significant advantages over the AB_5s in cost, especially if the A-element is mostly Ti and not Zr. Also, if alloys contain V, they should also have some Fe present to allow the use of low-cost ferrovanadium (used by the steel industry). AB_2s seem to be relatively sensitive to impurities in the hydrogen, although little good quantitative data exist. The commercial production of AB_2 compounds tends to be more difficult than AB_5 compounds. [4]

1.3.3 AB Intermetallic Compounds

The AB family of alloys is primarily based upon TiFe and its substitutional modifications (Mn or Ni in place of Fe). They tend to have two plateaus (two distinct hydrides), both with reasonable pressures at ambient temperature. The PCT properties can be tuned somewhat with substitution for Ti and Fe. H-capacities are competitive with the best of the AB_5s and AB_2s, and they also have a low cost. However, hysteresis tends to be on the high side, and they are sensitive to gaseous impurities in the hydrogen used. Cyclic stability of the lower plateau is excellent, but the upper plateau tends to drift higher and higher with cycling, ultimately rendering it unusable. The problems associated with gaseous impurities and upper plateau instabilities have prevented large scale commercial use of the AB alloys. [4]

1.4 Metal Hydride Modelling Literature Review

In order for metal hydride hydrogen storage systems to compete with existing energy storage technology, such as gasoline tanks and batteries, it is important to have quick refuelling and discharging rates. Improving the reaction rates involves enhancing the heat transfer rate within the reaction bed. There are a number of enhancements that can be made to improve the heat and mass transfer. To complement experimental investigations, a mathematical model can be developed to describe the heat and mass transfer phenomena within the reaction bed and to study the influence of heat and mass transfer enhancements. This section describes some of the past work involving the modelling of metal hydride canisters.

One of the earlier metal hydride models is that of Mayer *et al.* [5], created in 1987. They developed a one-dimensional model capable of describing the transient heat and mass transfer within metal hydride reaction beds. Some of the most important contributions from their work are the rate equations describing the rate at which hydrogen is either absorbed or desorbed from the metal hydride. They determined the rate expressions experimentally using a specially designed heat-pipe-cooled fast reactor [6]. These rate expressions are still used today in many metal hydride models. Mayer *et al.* used the finite difference method to solve the coupled equations. They found that their modelled transient behaviour of reaction beds (pressure, temperature, and concentration) showed very good agreement with experimental data.

Sun *et al.* [7] felt that models with constant hydrogen and metal hydride physical properties could not reflect practical cases well. Thus, they developed a one-dimensional model in 1988 [7] which includes the effects of the effective thermal conductivity in the hydride bed (as a function of pressure and hydrogen concentration), and the effects of varying the physical properties of the metal hydride and other operating parameters. In 1989 [8] they developed a two-dimensional model as an extension of their one-dimensional model, which includes the general equations for effective thermal conductivities in hydride beds, pressure-concentration-temperature (P-C-T) curves, and hydriding or dehydriding kinetics of metal hydrides, thus making their new model "more universal" [8]. Their two-dimensional model is validated against experimental results, and shows good agreement; however they do not compare models with constant properties and varying properties to experimental results to see if the models with varying properties are more accurate. Typically any additional relations that add complexity to the mathematical model should be checked to see if they add enough accuracy to warrant the additional time spent numerically solving the problem. In 1990 [9], Sun *et al.* describe their model in more detail, and show a numerical solution based on finite difference approximations where the alternating-direction implicit method is used. Their model shows good agreement with their experimental results, for transient dehydriding behaviour of an $MlNi_{4.5}Mn_{0.5}$ (Ml stands for lanthanum-rich misch metal) cylindrical reaction bed. In 1992 [10], Sun performed a study to design optimal metal hydride reactors based upon the mathematical model. He found that the thickness of the hydride bed is the most important design parameter. An annular reactor with internal horizontal fins, shown in Figure 1.2 as 011, was found to yield the highest reaction rate, when compared with other internally finned geometries shown in Figure 1.2 as 010 and 101.

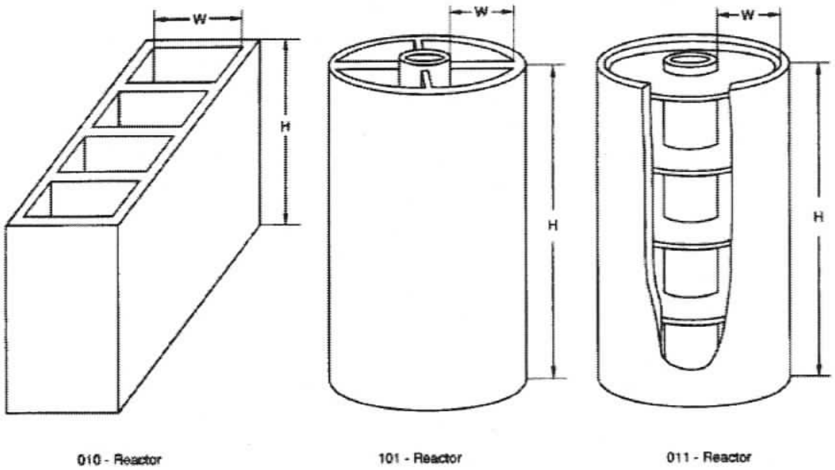

Figure 1.2 – Configurations of metal hydride reactors with internal fins. [10]

Ram Gopal *et al.* [11] created a one-dimensional model in 1992 for heat and mass transfer in metal hydride beds of annular cylindrical configuration. They argued that previous models were limited to specific alloys only, and that generalized studies which facilitate the prediction of performance of different alloy systems were not available [11]. Thus, they developed a one-dimensional model in dimensionless form, covering a wide range of alloys and operating conditions. They concluded, as most studies do, that the rate-controlling resistance to heat and mass transfer is the thermal resistance offered by the metal hydride bed, and the best way of designing reactors is to improve the heat transfer characteristics by keeping the bed thickness as small as possible and improving the conductivity of the bed. In 1993 [12], they developed a one-dimensional model. To ensure that their analysis was a generalised one they grouped the input and output variables into non-dimensional parameters. They also varied the significant metal hydride properties and operating conditions over a large range so that the results could be applied to a variety of alloys and applications. Once again, they concluded that an improvement in the heat-transfer characteristics of the bed is most essential.

In 1995 Jemni and Ben Nasrallah [13] developed a numerical model for the two-dimensional transient heat and mass transfer during absorption within a metal hydride reactor. In this model they account for the difference between the solid and gas temperatures, as well as the variation of the gas pressure. The system of equations was resolved numerically by the finite domains method. They demonstrated the significance of two-dimensional effects for their chosen dimensions. They also concluded the thermal equilibrium assumption is not valid throughout the whole reactor (i.e. gas and solid temperatures must be modelled separately) and that the term of heat transport by convection can be neglected. In 1995 [14] they developed another two-dimensional model which simulates desorption instead of absorption. Everything about this model is the same as the first model, except for the reaction kinetics expression which describes desorption instead of absorption. Again they concluded that the thermal equilibrium assumption is not valid in the whole reactor, the term of heat transport by convection can be neglected, and that an increase in the effective thermal conductivity of the solid leads to significant improvement of performance for the reactor. In 1997 [15] they utilized their absorption and desorption models to test the validity of the following three hypotheses:

- The solid and the gas are at the same temperature (local thermal equilibrium).
- The effect of pressure variation in the reactor is negligible.
- The effect of the hydrogen concentration on the equilibrium pressure variation is negligible.

For a $LaNi_5$ reactor (primary AB_5 type alloy) they discovered that all three of these hypotheses are valid, including local thermal equilibrium, which is contrary to their papers in 1995. Formally validating these hypotheses was a helpful endeavour for metal hydride modelling. In 1999 [16] they published an experimental and theoretical study of a $LaNi_5$ reactor. In this study they set out to experimentally determine the effective thermal conductivity, the conductance between the hydride bed and the fluid around the reactor, the equilibrium pressure, and the expression of the reaction kinetics. They also tested the validity of their theoretical model by comparison between theoretical and experimental results. They derived an analytic expression of the equilibrium pressure and the reaction kinetics (for absorption and desorption), and values for the effective thermal conductivity and the conductance between the hydride bed and the fluid around the reactor. They also found good agreement between the experimental and the calculated results.

In 2001 [17], Mat and Kaplan modelled an $LaNi_{4.8}Sn_{0.2}$ storage tank. They adapted Jemni and Ben Nasrallah's mathematical model (described above) and applied it to experimental studies available in the literature to study the fundamental mechanisms of hydride formation and heat and mass transfer which takes place in the hydride bed. They found that the model successfully predicts similar temperature histories and hydride formation curves with the experiments considered. In 2005 [18] they were part of a team that presented another theoretical and experimental analysis of hydrogen absorption in $LaNi_5$ metal hydride tanks. They felt that there were very limited studies validating theoretical models and investigating various bed geometries on hydriding processes. Therefore, they studied theoretical and experimental hydrogen absorption and compared the behaviour of solid tanks to that of annular tanks. They found that their mathematical model adequately captures the main physics of the hydriding process and can be employed for a better hydride bed design to reduce hydriding time.

Nakagawa *et al.* [19] presented a two dimensional mathematical model of a metal hydride bed in 2000. They felt as though previous studies did not fully discuss the validity of the thermal equilibrium and negligible convection assumptions. It should be noted that they neglect to reference the appropriate Jemni and Ben Nasrallah studies that were discussed above when making this statement, although later in the paper they mention the appropriate study (their references section contains errors). They also stated that thermophysical properties such as thermal conductivity, specific heat, and particle diameter depend on the reacted fraction of hydride, and few studies take into account all of these. They also disapprove of models that describe reaction kinetics by simplified models such as the Arrhenius equation, and therefore decided to use a kinetic expression presented by Inomata *et al.* [20]. They discovered that the local thermal equilibrium assumption is not valid throughout the whole reactor. They note the difference between this result and that of Jemni and Ben Nasrallah, and state that the cause of the discrepancy is that they did not select an appropriate convection coefficient between the gas and solid phases. They also state that the convection term is significant up until a certain time. It should be noted that they do not appear to make any comparisons with experimental data to prove some of their strong claims.

Jiang *et al.* [21] described the behaviour of a thermally coupled metal hydride hydrogen storage and fuel cell system. They applied a new and unique approach by utilizing lumped approximations in a computational environment referred to as the virtual test bed. They modelled the dynamic performances of the metal hydride bed and fuel cell stack with enough rigor to capture the physics but not overwhelm the system simulator. They applied a pulsed electrical load to their system. Their study revealed unique and subtle behaviour associated with thermally coupled systems that could not be easily gleaned from simulating each device alone.

1.4.1 Weaknesses

Aside from the study performed by Jiang *et al.* [21] there has been little modelling work related to the thermal coupling of metal hydride storage systems to the energy conversion devices they are fuelling. With the emphasis of most metal hydride studies focusing on heat transfer improvements it is important to examine the impact of exploiting the readily available heat energy generated by the conversion device. Particularly, none of the models discussed above have been developed to explore the effect of different heat transfer enhancements and storage tank configurations with respect to a thermally coupled metal hydride and converter system.

Another limitation in the models described above is that they typically model either absorption or desorption and not both simultaneously. There are many applications where metal hydride tanks are not simply emptied in one continuous discharge, but rather there is dynamic behaviour associated with cyclic loads and varying external conditions. This is especially true when metal hydride storage systems are used to provide hydrogen for uninterruptible power supplies or small motorized vehicles such as scooters. Typical load patterns involve periods of use where varying load may be applied combined with down time where no load is applied and the hydrogen in the tank is allowed to settle. Dynamic behaviour may potentially vary significantly from continuous use especially if there is redistribution of hydrogen within the tank. In order to model cyclic behaviour appropriately it is beneficial to have a dynamic model capable of modelling both absorption and desorption simultaneously.

1.5 Thesis Objectives

For conventionally sized storage systems and usage patterns heat transfer is the rate limiting factor for absorption and desorption of hydrogen in metal hydride storage tanks. Therefore, it is beneficial to increase the rate of heat transfer to improve reaction rates (especially for reducing filling times).

In order to use engineering to enhance the design of storage tanks it is important to have a numerical model that can accurately describe the dynamic behaviour within a metal hydride tank. This reduces the reliance on experimental testing for new designs and facilitates innovation.

Metal hydride hydrogen storage systems are often used in conjunction with fuel cell systems or internal combustion engines. These converters usually have a waste exhaust stream at elevated temperatures. Since metal hydride tanks require heat in order to desorb hydrogen there is a potential to utilize waste heat from the fuel cell to enhance the desorption of hydrogen gas in the metal hydride tank.

Considering these points, there are three main objectives for this thesis:

- develop a comprehensive, two-dimensional model describing the behaviour in a metal hydride hydrogen storage tank under dynamic operating conditions;
- develop heat transfer relations that enable the metal hydride model to be coupled with a fuel cell system;
- examine the effects of heat transfer enhancements and storage tank configurations on a thermally coupled metal hydride hydrogen storage and fuel cell system.

2 Metal Hydride Heat Transfer Issues

As introduced in Chapter 1 metal hydride absorption and desorption reactions are exothermic and endothermic respectively. Unfortunately, most metal hydride powders have poor heat transfer coefficients and require engineering enhancements. Typically heat transfer is the rate limiting factor for absorption and desorption; therefore it is important to enhance the transfer of heat to the reaction zone in order to enhance metal hydride hydrogen storage systems. This chapter will discuss the impact of the heat transfer resistance due to the metal hydride bed with the use of a one-dimensional resistive network analysis, and describe the variation of this resistance as the tank empties.

A one-dimensional thermal analysis is performed to illustrate the relative importance and magnitude of the thermal resistances, and assess the possible impact of external fins on the overall heat transfer rate. This is done for two main cases, with two variations for each. The first case involves a metal hydride tank with no external heat transfer enhancements. The second case involves a metal hydride tank with evenly spaced fins on the exterior. Two variations for each of these cases are also analyzed: (a) the thermal circuit at the beginning of desorption (full tank); and, (b) the situation after two thirds of the hydrogen has been desorbed.

2.1 Resistive Network Analysis

In this analysis, a single metal hydride storage tank is examined. As shown in Figure 2.1, the storage system consists of an aluminum cylinder with a 24 cm length, 2 cm outer radius, and a wall thickness of 3.7 mm. The hydride material inside the tank is assumed to have the properties of $LaNi_5$. This tank size was selected because it is a good approximation of generic tank sizes, with a reversible hydrogen storage capacity of ~35g. $LaNi_5$ was selected as the alloy because it is a commonly used and well studied alloy making it appropriate for a general resistance investigation. Results presented are specific to this geometry and may not apply to tanks with significantly different aspect ratios.

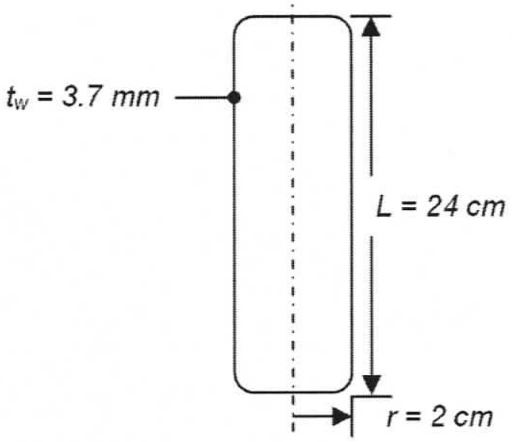

Figure 2.1 – Schematic of metal hydride tank used in resistive network analysis.

Because the tank has a high aspect ratio, the rate of heat transfer from the environment to the desorption site can be simplified and analyzed as a thermal circuit in the radial direction. Using an equivalent circuit analogy, the rate at which heat is transferred can be determined using,

$$q = \frac{\Delta T}{R_{t,tot}} \tag{2.1}$$

where the thermal resistances for conduction in the radial direction, surface convection, and for finned surfaces are given by the following equations [22]:

$$R_{t,cond} = \frac{\ln\left(r_2/r_1\right)}{2\pi kL} \tag{2.2}$$

$$R_{t,conv} = \frac{1}{h2\pi r_2 L} \tag{2.3}$$

$$R_{fin} = \left\{ hA_t \left[1 - \frac{NA_f}{A_t} \left(1 - \eta_f \right) \right] \right\}^{-1} \tag{2.4}$$

where r_2 and r_1 are the exterior and interior radii respectively, k is the thermal conductivity, L is the height of the tank, h is the convection coefficient, A_t is the total surface area of the tank (including fins), A_f is the surface area of a fin, N is the number of fins, η_f is the fin efficiency, and ΔT is the temperature difference. The external convection coefficient is assumed to be 150 W/m^{2}K.

It is important to note that when desorption is driven by an increase in external temperature, the reaction within the tank does not occur evenly throughout the hydride bed. During desorption, the reaction is highly endothermic and can only proceed in locations where there is an adequate heat source. Since, in this case, heat is provided through the exterior walls of the tank, modeling experience has shown that the reaction proceeds like a wave from the exterior to the interior of the tank. This behaviour is important because it creates a phenomenon whereby the thermal resistance of the circuit increases as the reaction proceeds due to the reaction location moving towards the tank centre. Thus, the resistance due to the alloy increases and becomes more significant depending on the state of charge. This phenomenon is described in more detail in Section 2.3.

2.1.1 Case 1a: No Fins/Start of Desorption

When the hydride tank is full, and the external temperature is increased, the initial resistance network is shown in Figure 2.2a. Heat is driven from the external fluid at T_∞ to the material near the tank wall, at $T_{w,i}$.

2.1.2 Case 1b: No Fins/Desorption Two-thirds Complete

Once the desorption process has proceeded far enough so that the alloy two-thirds of the distance from the tank wall has reacted, the resistance network can be drawn as in Figure 2.2b. This case assumes that the hydride material near the wall is depleted and that the desorption reaction is occurring near the centre of the tank.

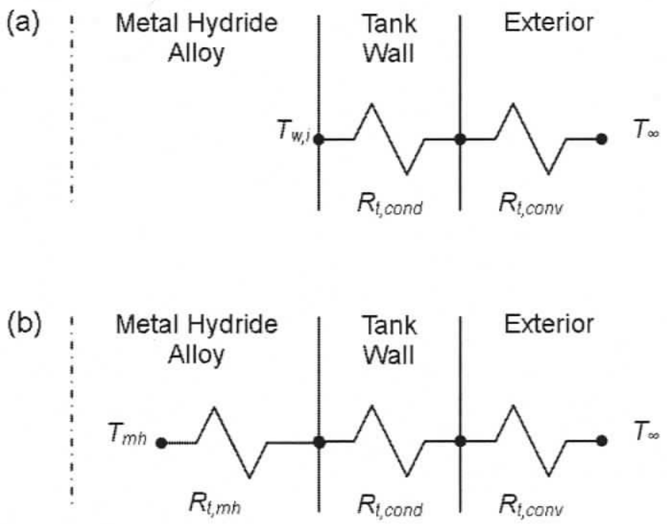

Figure 2.2 – (a) Schematic of resistance network for Cases 1a and 2a. (b) Schematic of resistance network for Cases 1b and 2b.

2.1.3 Case 2a: With Fins/Start of Desorption

For the second case studied, it is assumed that the tank now has a finned structure on the outer radius. The layout and dimensions of the finned tank are shown schematically in Figure 2.3. The number of fins on the tank surface is assumed be 50, and the convection coefficient is assumed to be the same as for Case 1.

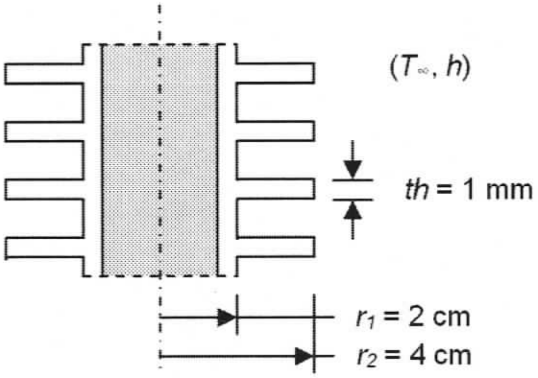

Figure 2.3 – Cross section of the metal hydride vessel showing the external fin structure used in calculations.

2.1.4 Case 2b: With Fins/Desorption Two-thirds Complete

The final scenario examined is similar to Case 1b where it is assumed the desorption reaction has proceeded so that only the inner third of the alloy is still charged with hydrogen. The resistance network for this scenario is shown in Figure 2.2b. In this case, the external resistance is due to the finned structure. The effective resistance is calculated using Eq. (2.4).

2.1.5 Resistive Network Analysis Results

For the four scenarios described above, the thermal resistances for each component are calculated using the respective geometry, convection coefficient, and material properties. The calculated resistances are displayed in Figure 2.4. The resistance due to the aluminum tank wall is approximately three orders of magnitude lower than the other resistances and is therefore negligible.

The results in Figure 2.4 show that a finned surface decreases the thermal resistance nearly an order of magnitude at the beginning of desorption, whereas, when the reaction has proceeded through two-thirds of the bed, the fins have much less impact on the overall thermal resistance. At this point, the reacted metal hydride alloy has become the dominant resistance.

These results suggest that there is a potential for external fins to make a significant contribution to the overall heat transfer of the storage system. The impact of external fins on a thermally coupled metal hydride hydrogen storage and fuel cell system will be investigated in more detail by a two-dimensional model and discussed in Chapter 6.

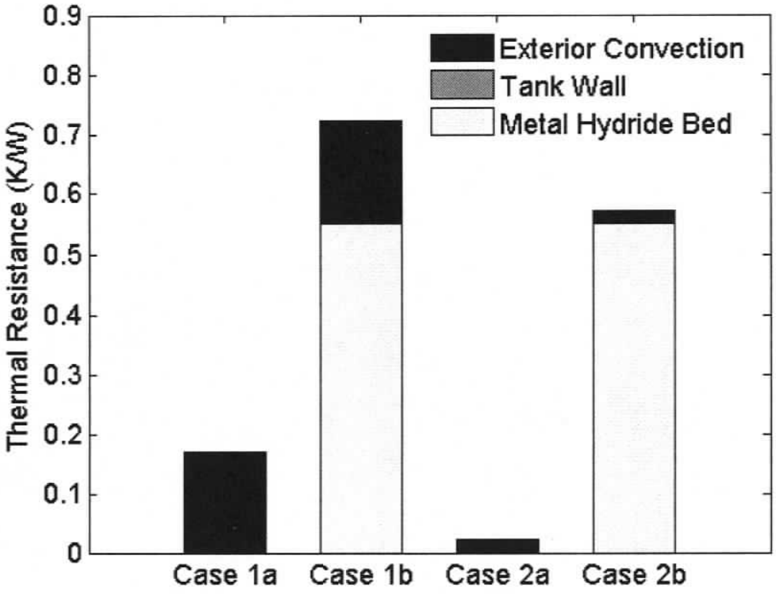

Figure 2.4 – Results of the thermal circuit analysis.

2.2 Overview of Metal Hydride Bed Resistance

In order to place these results in context the overall impact of the metal hydride bed on the heat transfer of the system as the tank empties will be described here. The following example will consider the desorption of a metal hydride tank that is initially full of hydrogen and is emptied at a constant rate. In order to initiate desorption heat is applied at the external tank walls. Initially, the metal hydride alloy immediately adjacent to the walls is full of hydrogen; therefore as the heat is applied the alloy will desorb hydrogen.

It should be noted that this reaction consumes the energy that is being applied to liberate the hydrogen; therefore only the alloy that is immediately adjacent to the wall can react since the rest of the alloy within the tank receives no heat. As time passes, the alloy that is reacting desorbs all of its hydrogen and the heat is allowed to travel towards the centre of the tank. The region of metal hydride alloy that is desorbing hydrogen is referred to as the *reaction zone*. As the tank empties, the reaction zone propagates like a wave from the exterior walls (where the heat is applied) towards the centre region of the tank. When the reaction zone is adjacent to the tank walls the heat transfer only encounters resistance due to the tank wall, which is usually made from a highly conductive material and is therefore negligible. However, as the reaction propagates towards the centre of the tank the heat transfer encounters increasing resistance because it must travel through the depleted alloy to reach the reaction zone. Contrary to the tank wall material metal hydride powders tends to have very low thermal conductivity values. Therefore, as the tank empties the amount of thermal energy that reaches the reaction zone is usually significantly reduced. The tank therefore experiences a reduction in the rate of the desorption reaction. This typically manifests itself as a reduction in the outlet pressure of the hydrogen gas stream for a fixed hydrogen flow rate, when a constant heat source is applied. Since metal hydride hydrogen storage systems often supply hydrogen for fuel cell systems that have minimum inlet pressure requirements, it is important to maintain high pressures as the hydride tanks are emptied. This phenomenon must be kept in mind when designing heat transfer enhancements for metal hydride systems.

3 Metal Hydride Model

3.1 Assumptions

The following assumptions are used in formulating the metal hydride model.

1. Symmetry along the centre line of the tank allows the system to be modelled as a two-dimensional axi-symmetric domain.
2. The solid and the gas are at the same temperature (local thermal equilibrium),
3. The effect of pressure variation in the tank is negligible.
4. The effect of the hydrogen concentration on the equilibrium pressure variation is negligible (flat desorption and absorption plateaus on the P-C diagram).
5. Heat transport by convection is negligible.
6. The advection terms in the energy equation can be neglected.
7. Hydrogen gas behaves as an ideal gas.
8. The thermal mass of the fins themselves is assumed to be negligible.

The first assumption adequately approximates the physical scenario being modelled here since there is likely to be little variation in the convection coefficient or temperature values along the perimeter of the exterior tank walls. Assumptions two through four are validated by Jemni and Ben Nasrallah [15] as noted above. Assumption five was explicitly validated by Jemni and Nasrallah [13,14], but it is also a result of assumption three, since heat transport by convection is directly related to the pressure variation in the reactor. Assumption six is also a result of assumption three since a negligible pressure gradient results in insignificant gas velocity through the tank, thus resulting in negligible advection terms. Assumptions seven and eight are commonly used assumptions and are appropriate for the purposes of this study.

3.2 Governing Equations

Assuming thermal equilibrium between the metal hydride alloy and hydrogen gas, a single energy equation can be used. For a two-dimensional (axi-symmetric) scenario, with r and z axes, the energy equation is:

$$\left(\rho c_p\right)_e \frac{\partial T}{\partial t} = \frac{1}{r}\frac{\partial}{\partial r}\left(r k_e \frac{\partial T}{\partial r}\right) + \frac{\partial}{\partial z}\left(k_e \frac{\partial T}{\partial z}\right) - m\left(\Delta H + T\left(c_{pg} - c_{ps}\right)\right) \tag{3.1}$$

where k_e, , ΔH, c_{pg}, c_{ps}, and m are effective thermal conductivity of the hydride bed, the enthalpy change of the hydriding reaction, specific heat of the gas and solid phases respectively, and the rate of hydrogen mass absorbed per unit volume. The m term accounts for both absorption and desorption, but as it is used in this thesis the positive form of m represents absorption, and negative form represents desorption. The $(\rho c_p)_e$ term is the volume averaged heat capacity of the gas and solid and is given below as Eq. (3.7).

The gas velocity within the reactor can be calculated using Darcy's law:

$$V_g = -\frac{K}{\mu_g}\nabla P_g \tag{3.2}$$

where K, μ_g, and P_g are the permeability of the porous medium, the dynamic viscosity of hydrogen, and the pressure of the hydrogen gas respectively.

The mass balance expression for hydrogen gas is:

$$\varepsilon \frac{\partial\left(\rho_g\right)}{\partial t} + \nabla \bullet \left(\rho_g V_g\right) = -m \tag{3.3}$$

where ε is the porosity of the metal hydride bed, ρ_g is the density of the hydrogen gas, and the m term is the rate of hydrogen mass absorbed per unit volume, as noted above for the energy equation. When solving this equation the hydrogen is assumed to be an ideal gas.

Assuming the solid volume is fixed, the mass balance for the solid is:

$$(1-\varepsilon)\frac{\partial(\rho_s)}{\partial t} = m \tag{3.4}$$

where ρ_s is the density of the metal hydride alloy.

The expression for the rate of hydrogen absorbed per unit volume is [5]:

$$m_{abs} = C_a \exp\left(-\frac{E_a}{R_g T}\right)\ln\left(\frac{P_g}{P_{eqa}}\right)(\rho_{sat} - \rho_s) \tag{3.5}$$

where C_a is the absorption constant, E_a is the activation energy for absorption, P_{eqa} is the equilibrium pressure for absorption, and ρ_{sat} is the density of the metal hydride alloy when it has absorbed all of the hydrogen gas that can reversibly be absorbed. The equation for the equilibrium pressure is given below as Eq. (3.10). Adopted from [13], C_a is equal to 59.187 1/s and E_a is equal to 21,179.6 J/mol. It should be noted that these values are for the metal hydride alloy $LaNi_5$. However, because heat transfer is the rate limiting factor, and metal hydride alloys have similar reaction rates, these values are a good approximation for other metal hydride alloys.

The expression for the rate of hydrogen desorbed per unit volume is [5]:

$$m_{des} = C_d \exp\left(-\frac{E_d}{R_g T}\right)\left(\frac{P_g - P_{eqd}}{P_{eqd}}\right)(\rho_s - \rho_{emp}) \tag{3.6}$$

where C_d is the desorption constant, E_d is the activation energy for desorption, P_{eqd} is the equilibrium pressure for desorption, and ρ_{emp} is the density of the metal hydride alloy when it has desorbed all of the hydrogen gas that can reversibly be desorbed. The equation for the equilibrium pressure is given below as Eq. (3.10). Adopted from [14] C_d is equal to 9.57 1/s and E_d is equal to 15,473 J/mol. The same is true for these values as noted above for the absorption rate expression.

These two expressions have been combined in the model by allowing the final m term to assume the value of either m_{abs} or m_{des}. The logical statements that have been applied to Eq. (3.5) and Eq. (3.6) allow for only one of m_{abs} or m_{des} to have a local value other than zero. The m term will assume the value of whichever one is not zero, if both are zero then the m term will also be zero. If m_{des} is used, a negative value is generated since the governing equations are formulated to consider a positive m term as absorption.

This allows the model to simulate absorption and desorption simultaneously, which is essential because within the hydride bed there may be areas that are absorbing hydrogen locally while other areas are desorbing hydrogen. This is especially true of dynamic simulations where there may be rapid variations in hydrogen demands as well as pressure and external temperature.

From the energy equation, Eq. (3.1), the $(\rho c_p)_e$ term is calculated as:

$$(\rho c_p)_e = (\varepsilon \rho_g c_{pg} + (1-\varepsilon)\rho_s c_{ps}) \tag{3.7}$$

The ideal gas relation used to determine gas density is as follows:

$$\rho_g = \frac{M_g P_g}{R_g T} \tag{3.8}$$

The temperature dependent dynamic viscosity term is calculated using [24]:

$$\mu_g = 9.05\times10^{-6}\left(\frac{T}{293}\right)^{0.68} \tag{3.9}$$

The equilibrium pressure for absorption and desorption is calculated using the van't Hoff relationship:

$$\ln P_{eq} = A - \frac{B}{T} \tag{3.10}$$

where A and B for P_{eqa} and P_{eqd} are determined from the Hydride Material Listing Database [25]. The values used for A and B are summarized in Table 3.1 for the model validation simulations and Table 5.2 for the thermally coupled simulations. Hysteresis results in different values of A and B for P_{eqa} and P_{eqd}. Utilizing different equations for P_{eqa} and P_{eqd}, allows the model to more accurately represent the behaviour within the tank, because hysteresis is accounted for.

3.2.1 Implementation

The model is implemented using a program called COMSOL Multiphysics™. When solving partial differential equations, COMSOL Multiphysics™ uses the finite element method. Since the model for the dynamic conditions in a metal hydride canister requires time-dependent partial differential equations, a time-dependent solver is used.

The COMSOL Multiphysics™ software enables the implementation of the governing equations by entering each differential equation as a separate "*physics mode*" thereby allowing each one to have unique boundary and initial conditions. The first physics mode is governed by Eq. (3.1) and the state variable is T. The second physics mode is a combination of Eq. (3.2) and Eq. (3.3) and the state variable is P_g. The third and final physics mode is governed by Eq. (3.4) and the state variable is ρ_s. These expressions all have a common variable, m, in their source terms, which is generated by Eq. (3.5) and Eq. (3.6). Since these equations are not differential equations they do not require a separate physics mode, therefore they are solved globally as "subdomain expressions" and the solutions are available for all of the physics modes.

3.2.2 Initial Conditions

Initially the pressure, the temperature, and the metal hydride density in the tank are assumed to be constant, the tank is fully charged, and is in a state of equilibrium:

$$T(r,z,0)=T_i \tag{3.11}$$

$$P_g(r,z,0)=P_i \tag{3.12}$$

$$\rho_s(r,z,0)=\rho_i \tag{3.13}$$

The values used for the initial conditions are summarized in Table 3.2 for the model validation simulations, Table 5.3 for the base and finned cases, and Table 5.4 for the annular case.

3.2.3 Boundary Conditions

Top surface boundary conditions:

$$@\, z=z_{t1},\ P_g=P_t \text{ or } V_g=V_t \tag{3.14}$$

$$@\, z=z_{t2},\ T=T_t \text{ or } k_t\frac{\partial T}{\partial z}=q_t'' \tag{3.15}$$

Centre axis boundary conditions:

$$@\, r = r_{c1},\ P_g = P_c \text{ or } V_g = V_c \tag{3.16}$$

$$@\, r = r_{c2},\ T = T_c \text{ or } k_c \frac{\partial T}{\partial r} = q_c'' \tag{3.17}$$

Side surface boundary conditions:

$$@\, r = r_{s1},\ P_g = P_s \text{ or } V_g = V_s \tag{3.18}$$

$$@\, r = r_{s2},\ T = T_s \text{ or } k_s \frac{\partial T}{\partial r} = q_s'' \tag{3.19}$$

Bottom surface boundary conditions:

$$@\, z = z_{b1},\ P_g = P_b \text{ or } V_g = V_b \tag{3.20}$$

$$@\, z = z_{b2},\ T = T_b \text{ or } k_b \frac{\partial T}{\partial z} = q_b'' \tag{3.21}$$

Figure 3.1 illustrates the locations associated with the co-ordinates given above for the boundary conditions of a generic metal hydride tank. The reason for utilizing two different values for each surface (i.e. z_{t1} and z_{t2} for the top surface) is because of the possible inclusion of the tank walls. Since the energy equation is the only governing equation that is active in the tank wall subdomain, the energy-based boundary conditions require boundary conditions imposed on the exterior walls of the tank, whereas all of the other equations that are not active in the tank walls require boundary conditions imposed at the exterior of the metal hydride subdomain which is actually the interior of the tank walls. The values used in these boundary conditions are summarized in Table 3.2 for the model validation simulations, Table 5.3 for the base and finned cases, and Table 5.4 for the annular case.

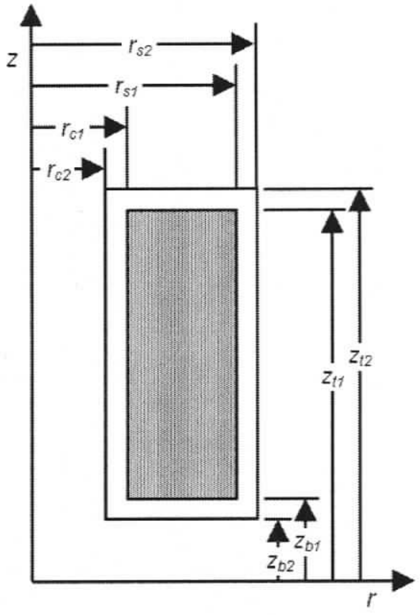

Figure 3.1 – Schematic of a generic metal hydride tank illustrating the co-ordinates for the boundary conditions.

3.3 Model Validation

With a mathematical model of a metal hydride tank developed, it is important to compare the model predictions to experimentally validated work. Since Jemni and Ben Nasrallah have done extensive modelling work [13-16] including experimental validation, and their models have been experimentally validated by other researchers [17] it would be valuable to compare the results from the model developed here with the results generated from their model. The reason for validating against experimentally validated model results and not directly against the experimental results is because the model results are more detailed, over a wider range, and based upon a scenario that is easy to duplicate, whereas the experimental results are usually much more limited with only a few data points, and performed under conditions that are not always easy to verify (i.e. whether or not the alloy is a pure version of what it is claimed to be). Therefore an accurate and detailed comparison can be accomplished by comparing the results of the model developed here to those of Jemni and Ben Nasrallah [13] for an $LaNi_5$ alloy undergoing absorption from a hydrogen source at a constant pressure of 1000 kPa with an exterior fluid temperature of

313 K. The metal hydride tank in this scenario has a radius of 5 cm, and a height of 3 cm. The properties of the $LaNi_5$ alloy used in the model are summarized in Table 3.1, and the initial and boundary conditions for this model are summarized in Table 3.2. A temperature comparison is shown in Figure 3.2 and a metal hydride density comparison is shown in Figure 3.3.

Table 3.1 - Properties of the metal hydride alloy $LaNi_5$.

Property	Metal ($LaNi_5$)
Saturated density, ρ_{sat} (kg m^{-3})	8527
Empty density, ρ_{emp} (kg m^{-3})	8400
Specific heat, C_p (J kg^{-1} K^{-1})	419
Effective thermal conductivity, k_e (W m^{-1} K^{-1})	1.32
Permeability, K (m^2)	10^{-8}
Reaction heat of formation, ΔH (J kg^{-1})	-1.539×10^7
Porosity, ε	0.50
A (for P_{eqa} in Eq. (3.10))	17.738
B (for P_{eqa} in Eq. (3.10))	3704.6
A (for P_{eqd} in Eq. (3.10))	17.608
B (for P_{eqd} in Eq. (3.10))	3704.6

Table 3.2 – Initial and boundary conditions for the model validation.

Variable	Value
T_i	290 K
P_i	1000 kPa
ρ_i	ρ_{sat}
z_{t1}	3 cm
z_{t2}	3 cm
V_t	0 m s^{-1}
k_t	k_e
q''_t	$h_f\left(T-T_f\right)$
r_{c1}	0 cm
r_{c2}	0 cm
V_c	0 m s^{-1}
q''_c	0 W m^{-2}
r_{s1}	5 cm
r_{s2}	5 cm
V_s	0 m s^{-1}
k_s	k_e
q''_s	$h_f\left(T-T_f\right)$
z_{b1}	0 cm
z_{b2}	0 cm
P_b	1000 kPa
T_b	290 K
h_f	2500 W m^{-2}K^{-1}
T_f	313 K

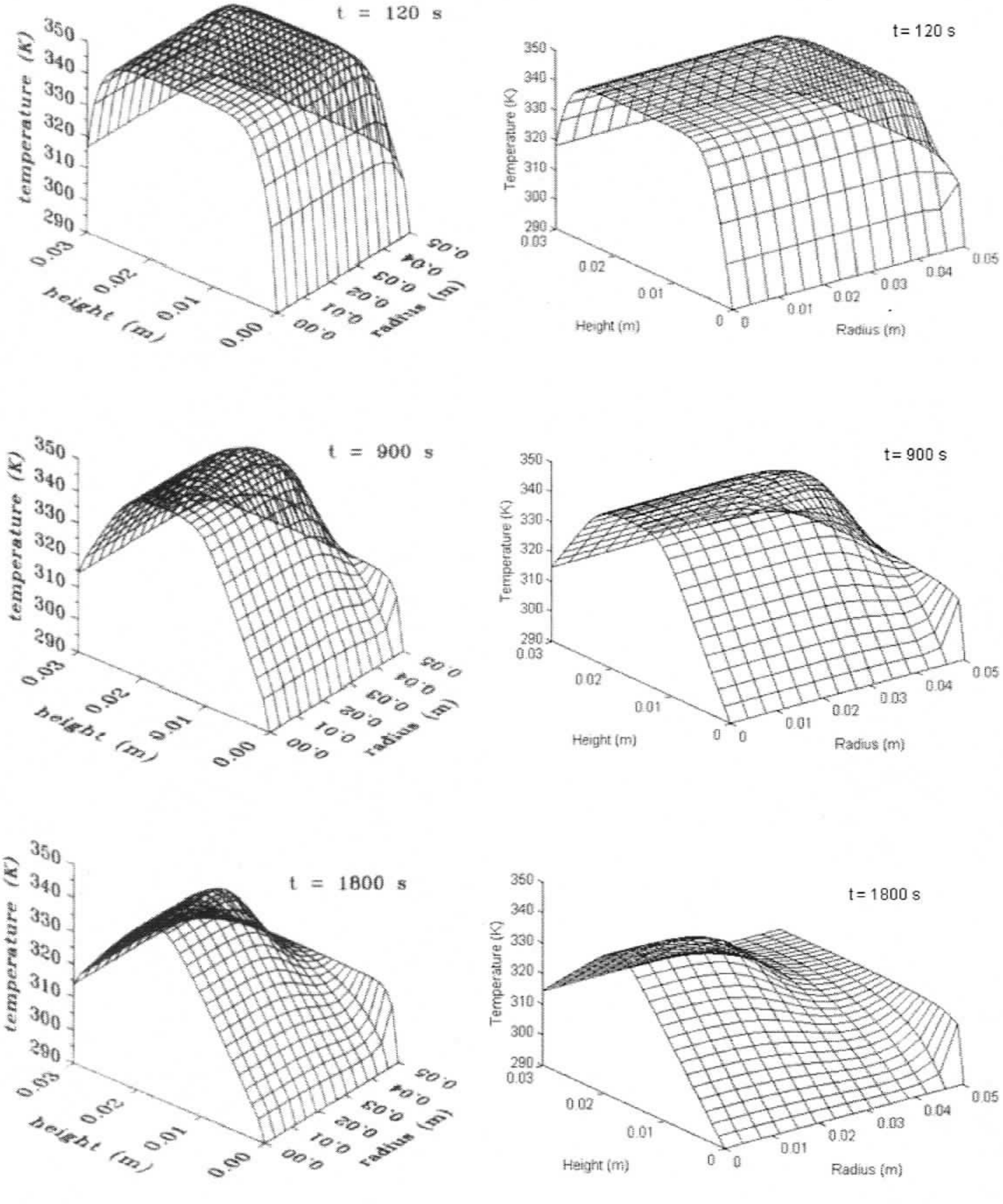

3.2a

3.2b

Figure 3.2 – Time-space evolution of temperature: (a) from the model developed by Jemni and Ben Nasrallah [13], and (b) from the model developed here.

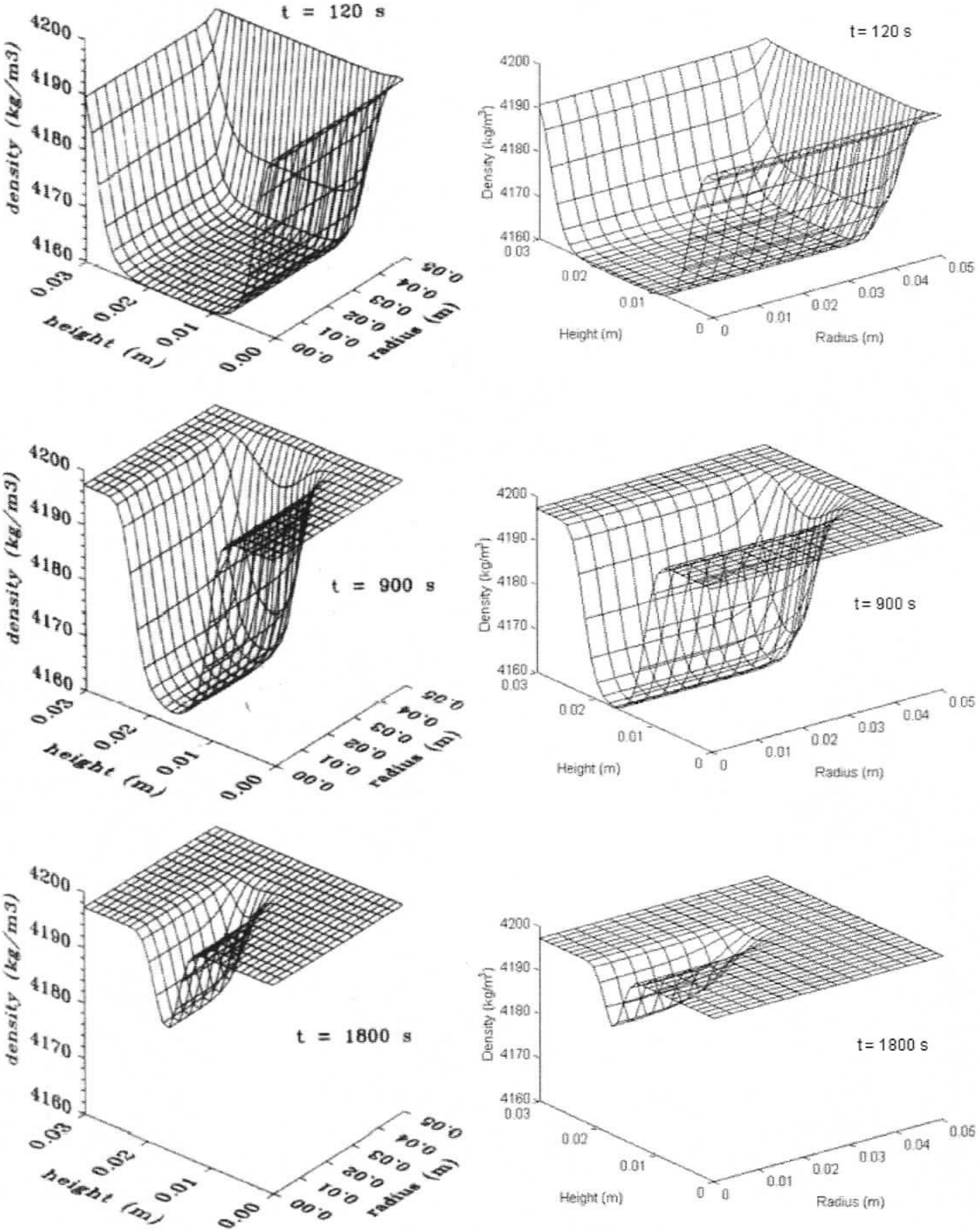

3.3a

3.3b

Figure 3.3 – Time-space evolution of metal hydride density: (a) from the model developed by Jemni and Ben Nasrallah [13], and (b) from the model developed here.

It can be seen from Figure 3.2 and Figure 3.3 that there is good agreement between the results of the model generated here and the results generated by the model of Jemni and Ben Nasrallah [13]. It should be noted that the perspective of the graphs is different, but nonetheless the values and shapes are the same. Also of note is that the model developed by Jemni and Ben Nasrallah includes separate energy equations for the gas and the solid (i.e. the local thermal equilibrium assumption was not used), the advection and heat transport by convection terms were included in the energy equations, and an equilibrium pressure relationship that is a function of the hydrogen concentration was used (i.e. the flat plateau slope assumption was not used). In spite of the fact that these assumptions were not made by Jemni and Ben Nasrallah in their earlier model [13] but they were made in the model developed here, the model results still show good agreement indicating that these assumptions are indeed valid. Now that the model has been validated it can be utilized to investigate heat transfer enhancements for a thermally coupled metal hydride hydrogen storage and fuel cell system.

4 System Configuration

As mentioned previously in Chapter 1 there is a potential for realizing improvements in performance of metal hydride hydrogen storage systems by thermally coupling them to the converter being fuelled. The energy converters usually have a waste exhaust stream at elevated temperatures. Since metal hydride tanks require heat in order to desorb hydrogen there is a potential to utilize waste heat from the fuel cell to enhance the desorption of hydrogen gas in the metal hydride tank. This chapter describes the system being investigated for this thesis. The focus of this thermal coupling work is to determine the impact of heat transfer enhancements and storage tank configurations on a thermally coupled metal hydride and fuel cell system.

4.1 Fuel Cell

The fuel cell selected for this study is the BALLARD® Nexa™ power module. The Nexa™ is a commercial proton exchange membrane (PEM) fuel cell system capable of 1200 W peak power. For this study, it is assumed that the system is servicing an intermittent load cycling at levels of 0 and 50% power with a 30 minute period. The complete load profile is thus 600 W of power for 15 minutes (*on-cycle*), shut-off for 15 minutes (*off-cycle*), and repeated for 5 complete cycles. The fuel cell is supplied hydrogen from two metal hydride canisters; therefore, the hydrogen demand is assumed to be equally divided between each tank. The hydrogen mass flow associated with this load is illustrated in Figure 4.1 along with the state of fill of each hydride tank over the 2.5 hours of pulsed operation. The hydrogen demand oscillates between zero and a constant flow of 4.329×10^{-6} kg/s and when the simulation ends the storage tank is approximately 89% empty. The waste heat provided by the Nexa™ module for a 600 W load is 550 W [26].

The metal hydride tanks are thermally coupled to the fuel cell system by placement immediately above the vertical cooling channels, and additional duct work is used to ensure the waste heat air stream passes over the desired region or through the tank as required for each particular case. Figure 4.2 shows the arrangement of the tanks relative to the fuel cell, and Figure 4.3 shows the ducting work associated with the cases where the air flows over the exterior of the tanks. For the annular tanks, it is assumed that a collection manifold routes the exhaust gas through the inside of the storage tanks.

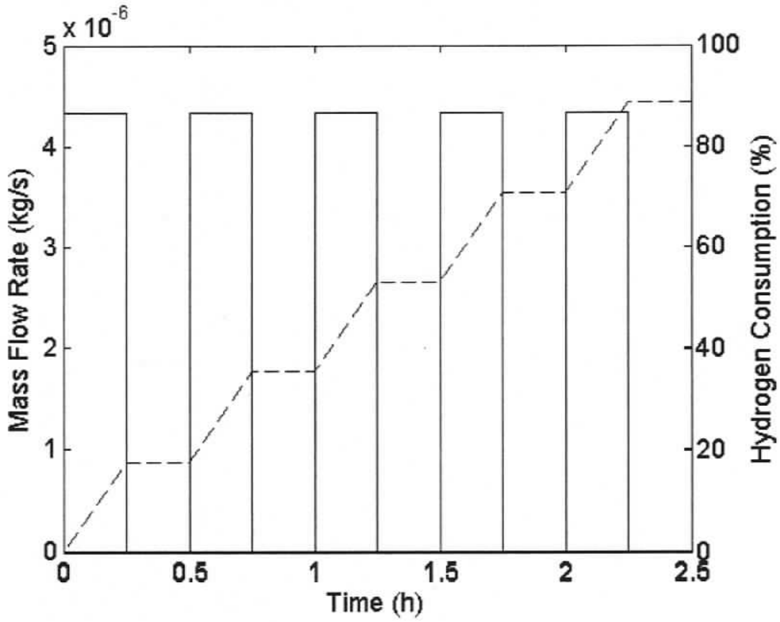

Figure 4.1 – Hydrogen mass flow rate exiting the tank and cumulative percentage of hydrogen in the metal hydride bed consumed over the 2.5 hours of pulsed operation.

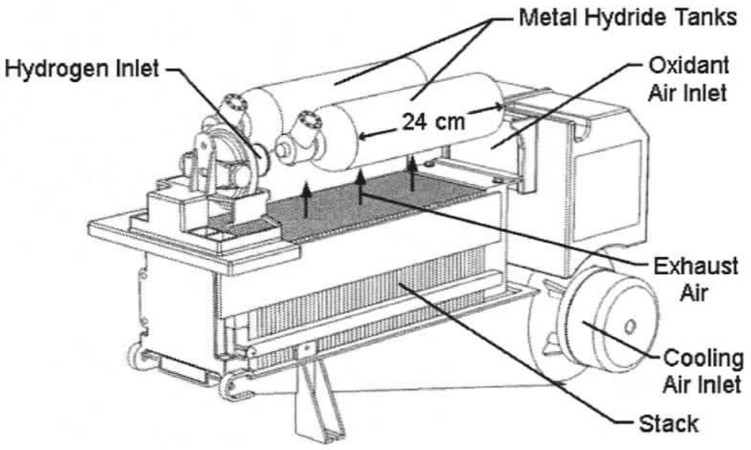

Figure 4.2 – Schematic of the system configuration illustrating the placement of two metal hydride tanks above the fuel cell's vertical cooling channels.

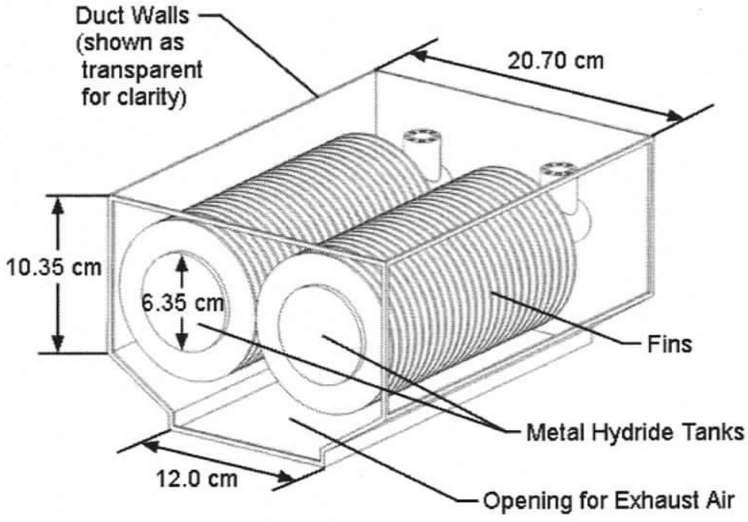

Figure 4.3 – Schematic of the ducting required for the finned configuration. (Note: not all fins are shown.)

4.2 Metal Hydride Alloy

When selecting a metal hydride alloy for a particular application the primary concern is usually the hydrogen pressure output at the desired operating temperature. Since the Nexa^{TM} module requires a minimum inlet pressure of 170kPa (absolute) [26], an alloy should be selected with an equilibrium desorption pressure that is significantly greater than 170 kPa for the lowest potential operating temperature (assumed to be ambient temperature at 25°C). The reason for a significantly greater desorption pressure at the operating temperature is to ensure that the system can maintain the minimum pressure while delivering hydrogen gas at the required flow rate. For this study, a commercially available AB_2 type alloy is selected with properties that are similar to the alloy used by Ovonic Hydrogen Systems LLC in their commercial storage systems. The exact composition of the alloy used in their hydride products is not known, so $Ti_{0.98}Zr_{0.02}V_{0.43}Fe_{0.09}Cr_{0.05}Mn_{1.5}$ is selected based upon similar equilibrium isotherms of the alloy. The properties for this material are obtained from Sandrock [4]. The alloy has sufficiently high pressures in the ambient temperature range (~1137 kPa), a hydrogen storage capacity of 1.9 wt%, and is inexpensive (~$6 CAD/kg) [4]. The size of the tanks is based upon the 20G250B model that is sold by Ovonic Hydrogen Systems LLC, which has a hydrogen capacity of 22 g, a diameter of 6.35 cm, and an approximate height of 26.5 cm including the valve [27].

4.3 Heat Transfer Enhancements

In order to compare different heat transfer enhancements applied to the system, three different cases are simulated. The first case is the base case, where no heat transfer enhancements are used. For the second case, the tank has 50 external fins of 2 cm length and 1 mm thickness attached on the circumference. The third case is an annular tank design where the air stream is piped directly through the centre of the tank. The annular geometry has an equivalent alloy content as the base case, but has a smaller overall diameter than the finned tank. These heat transfer enhancing designs were selected with the aim of investigating simple improvements that are easy to manufacture. Therefore the designs limit the use of internal structures, especially complex internal fin structures. Figure 4.4 shows a cross section of each of the three cases with the corresponding outer diameters. Since both tanks in each scenario operate under similar conditions, the numerical model simulates one tank utilizing half of the waste heat air stream from the fuel cell.

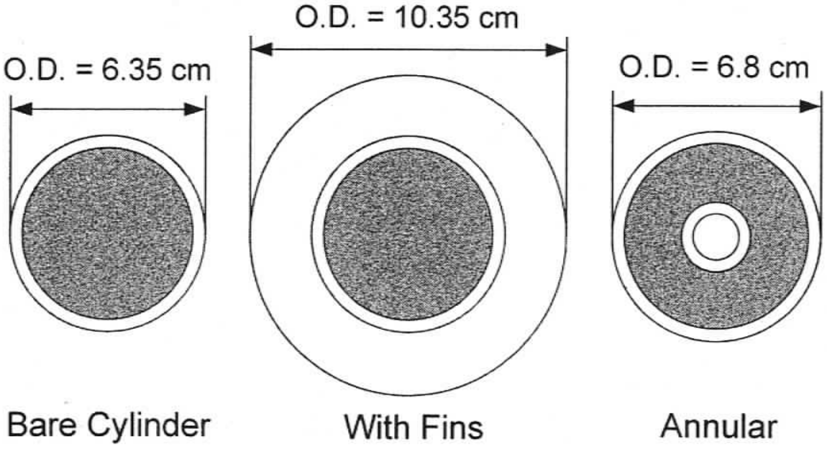

Figure 4.4 – Cross section of the metal hydride vessels for each of the three cases being studied, including a comparison of the outer diameter for each case.

5 Thermally Coupled System Modelling

5.1 Metal Hydride Model

The metal hydride storage system is modeled as a two-dimensional axi-symmetric system as shown in Figure 5.1 for the base and finned cases, and Figure 5.2 for the annular case. The geometry used in the model is based on the tanks described above in Chapter 4. Due to symmetry at the centre of the tank, the governing equations are solved for the r and z directions only. Two subdomains are included in addition to the subdomain representing the metal hydride alloy. The first subdomain simulates the tank walls, which are assumed to be 2024 T6 aluminum (properties are summarized in Table 5.1). This two-dimensional subdomain is shown in Figure 5.1 and Figure 5.2 as the unshaded region around the exterior of the metal hydride alloy (shaded region). The second subdomain accounts for the transient and spatial variation of the temperature of the exhaust air stream as it passes through the interior tube of the annular case. This one-dimensional subdomain is implemented along the left-hand side of the wall in Figure 5.2, at $r = 0.74$ cm. The subdomain for the metal hydride is the shaded region in Figure 5.1 for the base and finned cases, and Figure 5.2 for the annular case. All of the following governing equations are active in the metal hydride subdomain, in the tank wall subdomain only the energy equation is active. For the base and finned cases the outer tank radius is 3.175 cm, the height is 24 cm, and the thickness of the aluminum is 4 mm. For the annular case the outer tank radius is 3.4 cm, the radius of the internal opening is 0.74 cm, the height is 24 cm, and the thickness of the aluminum is 4 mm.

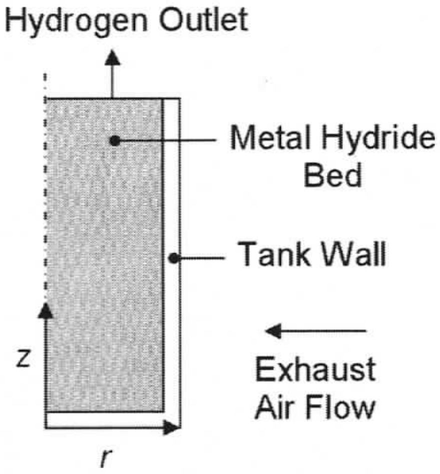

Figure 5.1 – Schematic of metal hydride tank used in mathematical model for the base and finned cases.

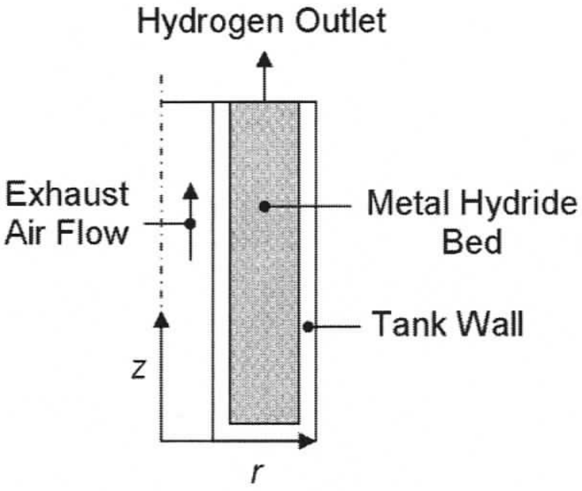

Figure 5.2 – Schematic of metal hydride tank used in mathematical model for the annular case.

Table 5.1 - Properties of the tank wall material, aluminum 2024-T6 [22].

Parameter	Value
Density, ρ (kg m^{-3})	2770
Specific heat, c_p (J kg^{-1} K^{-1})	875
Thermal conductivity, k_{Al} (W m^{-1} K^{-1})	177

The metal hydride is assumed to be $Ti_{0.98}Zr_{0.02}V_{0.43}Fe_{0.09}Cr_{0.05}Mn_{1.5}$ and the important properties of this alloy are summarized in Table 5.2. The properties are assumed to be constant throughout the 2.5 hours of operation. This alloy is assumed to have flat absorption and desorption plateaus on the P-C diagram, and the middle value is used in the equations. Hysteresis is included in the model by utilizing two distinct equations for the absorption and desorption pressures. Table 5.3 summarizes the initial and boundary conditions used for the base and finned cases and Table 5.4 summarizes the initial and boundary conditions used for the annular case. The h_{side}, T_{side}, T_{air}, h_{si}, and $T_{si}(z)$ variables are dependent on the waste heat exhaust stream provided by the fuel cell and are derived in Section 5.3. Since only the energy equation is active in the tank wall, the heat transfer boundary conditions are applied at the exterior of the tank, whereas all of the other boundary conditions are applied at the exterior of the metal hydride subdomain.

Table 5.2 - Properties of the metal hydride alloy, $Ti_{0.98}Zr_{0.02}V_{0.43}Fe_{0.09}Cr_{0.05}Mn_{1.5}$.

Parameter	Value
Saturated density, ρ_{sat} (kg m^{-3})	5577
Empty density, ρ_{emp} (kg m^{-3})	5500
Specific heat, c_{ps} (J kg^{-1} K^{-1})	490
Effective thermal conductivity, k_e (W m^{-1} K^{-1}) [assumed]	1.4
Permeability, K (m^2) [assumed]	10^{-8}
Reaction heat of formation, ΔH (J kg^{-1})	-1.359×10^7
Porosity, ε [assumed]	0.50
A (for P_{eqa} in Eq. (3.10))	18.789
B (for P_{eqa} in Eq. (3.10))	3295.6
A (for P_{eqd} in Eq. (3.10))	18.089
B (for P_{eqd} in Eq. (3.10))	3295.6

Table 5.3 – Initial and boundary conditions for the base and finned cases.

Variable	Value
T_i	T_∞ (298.15 K)
P_i	$P_{eqd}(T_\infty)$ (~1137 kPa)
ρ_i	ρ_{sat}
z_{t1}	24 cm
z_{t2}	24 cm
V_t	$\dfrac{G}{\rho_g}$
q''_t	0 W m^{-2}
r_{c1}	0 cm
r_{c2}	0 cm
V_c	0 m s^{-1}
q''_c	0 W m^{-2}
r_{s1}	2.775 cm
r_{s2}	3.175 cm
V_s	0 m s^{-1}
k_s	k_{Al}
q''_s	$h_{side}\left(T_{side} - T_{air}\right)$
z_{b1}	0.4 cm
z_{b2}	0 cm
V_b	0 m s^{-1}
q''_b	0 W m^{-2}
G	1.7894 x 10^{-3} kg s^{-1}m^{-2}

Table 5.4 – Initial and boundary conditions for the annular case.

Variable	Value
T_i	T_∞ (298.15 K)
P_i	$P_{eqd}(T_\infty)$ (~1137 kPa)
ρ_i	ρ_{sat}
z_{t1}	24 cm
z_{t2}	24 cm
V_t	$\dfrac{G}{\rho_g}$
q''_t	0 W m^{-2}
r_{c1}	1.14 cm
r_{c2}	0.74 cm
V_c	0 m s^{-1}
k_c	k_{Al}
q''_c	$h_{si}\left(T_{si}(z)-T_{air}\right)$
r_{s1}	3.0 cm
r_{s2}	3.4 cm
V_s	0 m s^{-1}
q''_s	0 W m^{-2}
z_{b1}	0.4 cm
z_{b2}	0 cm
V_b	0 m s^{-1}
q''_b	0 W m^{-2}
G	1.7894 x 10^{-3} kg s^{-1}m^{-2}

5.2 Experimental Data

In order to accurately represent the coupling between the metal hydride tanks and the Nexa^{TM} module some experimental data is required. Some data is available for the Nexa^{TM} module running at rated output (1200 W). Since this study assumes operation of the Nexa^{TM} module at 50% power (600 W), experimental data is used to more accurately characterize the temperature of the exhaust air. The Nexa^{TM} module that was used for the experiments is a table-top version of the fuel cell (as opposed to the rack mount modules), and the date of manufacture is listed as October 2001.

The experiment involved the fuel cell started from off mode in equilibrium with the laboratory temperature and immediately set for an output load of 600 W. A thermocouple placed approximately 2 cm above the exhaust channels recorded air temperature while a sensor built into the fuel cell reported stack temperature. This experiment yielded a steady-state exhaust air temperature that is approximately 14°C above ambient temperature. The time to reach steady-state yielded a thermal time constant, τ_{on}, of ~120 s. The recorded data is plotted in Figure 5.3 as a dashed line.

After steady-state was reached the fuel cell was shut off, and the temperature of the fuel cell stack was recorded as it declined. This yielded a thermal time constant for the off-cycle, τ_{off}, of ~110 s. It can be seen from Figure 5.3 that the experimental curve for the off-cycle is not a smooth line, and there is a distinct plateau reached at approximately 200 s before the temperature continues to decay towards ambient temperature. This behaviour is caused by the "purge cycle" of the fuel cell. When the fuel cell is shut off after operating at sufficiently high power loads it enters into a "purge cycle" lasting a few minutes where the fuel cell is switched on and off and the blower is run at full speed. Presumably this cycle is used to remove excess hydrogen and water. Although the purge cycle is not modelled exactly, the anomalous plateau section is not too severe and the overall trend for the temperature during the off-cycle can be simulated with an exponential expression. This is explained in more detail in Section 5.3.

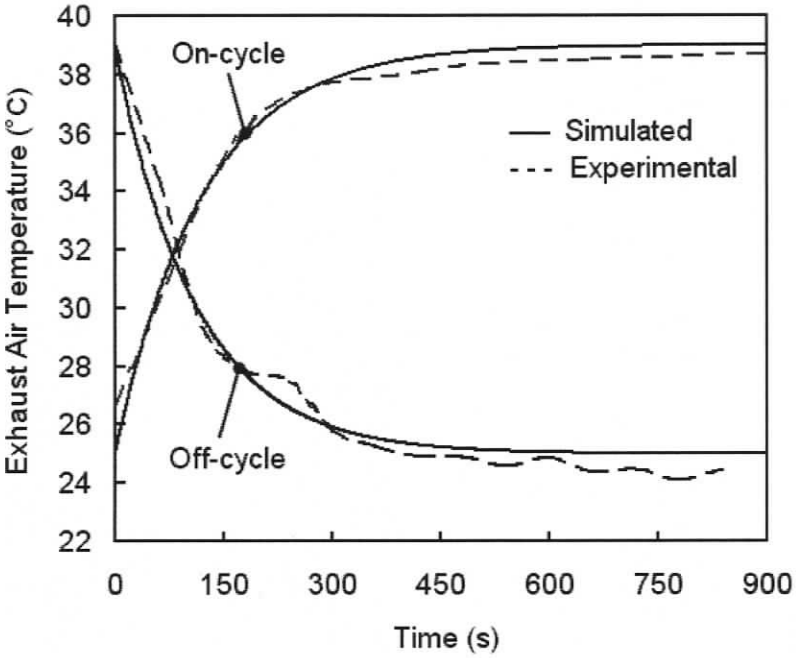

Figure 5.3 – Comparison of the simulated temperature expression used in the mathematical model with the experimental exhaust air temperature recorded from the Nexa^{TM} module for both the on and off cycles.

5.3 Heat Transfer Calculations

5.3.1 Assumptions

The thermal coupling between the fuel cell and the metal hydride tanks is a complex scenario which can be approximated by a series of relations describing air temperature and convection coefficients as a function of time. Many assumptions are required to allow for this scenario to be modelled while at the same time adequately representing a real-life application. The following assumptions are used in formulating the heat transfer relations.

1. For heat transfer to and from the metal hydride canisters it is assumed that radiation is negligible and heat transfer is due only to convection.

2. It is assumed that the exterior of the duct work is insulated and there is no heat transfer between the duct work and the surroundings.

3. For the cases involving ducted flow over the tank it is assumed that during the off-cycle the heat transfer from the exterior tank walls is due only to natural convection with air that is at ambient temperature.

4. It is assumed that because the tank is physically mounted by the top and bottom surfaces that these surfaces are insulated.

5. For the annular case it is assumed that the exterior tank walls are insulated.

6. During the off-cycle for the annular case it is assumed that the air through the interior channel is sufficiently quiescent such that a negligible amount of heat transfer occurs.

7. It is assumed that the exhaust air can be described by a first-order response function.

5.3.2 Fuel Cell Exhaust Air Temperature During the On-Cycle

In order to model the interaction between the tank and the external air flow, an expression describing the temperature of the exhaust air as it leaves the stack is required. Assuming the behaviour of the air temperature can be approximated as a first-order response function, the transient nature of the air temperature during operation can be described by the following equation:

$$\frac{T_a(t)-T_{ss}}{T_0-T_{ss}}=\exp\left(-\frac{t}{\tau_{on}}\right) \tag{5.1}$$

where T_0 is the initial temperature of the air at the start of each on-cycle, T_{ss} is the steady-state temperature (~39°C), t is time, and τ_{on} is the experimentally determined time constant for the on-cycle (~120 s). When these values are utilized, Eq. (5.1) yields a temperature behaviour that corresponds well to the experimental results. This can be seen in Figure 5.3 by comparing the simulated temperature curve with the experimental data.

To determine the amount of air flow exiting the fuel cell stack, a comparison is made between the temperature and flow rate values provided in the documentation for rated load versus the values experimentally determined at half load. At rated load (1200 W) and operating temperature the temperature of the exhaust air is listed as 17°C above ambient temperature, the max flow rate is listed as 3600 SLPM, and the waste heat is given as 1650 W [26]. At half-load the temperature difference is 14°C above ambient temperature, and the waste heat is listed as 550W. Not all of the waste heat is removed by the exhaust air stream, but using the given data and the measured temperatures, the heat absorbed by the air stream can be estimated. Performing an energy balance using the flow rate and temperature values at rated load yields a value of 1130 W for the heat removed by the air. Utilizing a ratio of actual waste heat (1650 W) and calculated amount of heat removed by the air (1130 W) for full load, the value of heat removed by the air at half load is determined to be 377 W assuming similar thermal behaviour at 50% load. An energy balance performed using this value and the experimental data from above yields a flow rate of 1450 SLPM for the exhaust air at half load.

5.3.3 Fuel Cell Exhaust Air Temperature During the Off-Cycle

With the exhaust air temperature of the on-cycle determined, the temperature drop during the off-cycle must now be determined. Once the fuel cell has been turned off and the purge cycle is completed, the exhaust fan no longer blows air through the cooling channels; therefore the air within the channels will experience minimal movement and is assumed to be quiescent. Because there is assumed to be no interaction between the fuel cell exhaust air and the metal hydride tanks during the off-cycle there is no need to determine the flow rate through the channels. However, in order to determine the initial temperature, T_0, that is to be used when the fuel cell is turned on again, the drop in air temperature while the fuel cell is turned off for 15 minutes must be determined. This temperature drop is due to the drop in stack temperature as it exchanges heat with its surroundings. The equation that describes the transient behaviour of the air temperature for the off-cycles is assumed to be similar to Eq. (5.1) (i.e. a first-order response function); however, the steady state temperature is now the ambient air temperature (~25°C):

$$\frac{T_a(t)-T_\infty}{T_0-T_\infty}=\exp\left(-\frac{t}{\tau_{off}}\right) \tag{5.2}$$

where T_∞ is the ambient air temperature, and τ_{off} is the experimentally determined time constant during the off-cycle (~110 s). As illustrated by Figure 5.3, the simulated temperature profile corresponds well to the experimental data. It is not necessary to implement this expression into the model because the air temperature reaches a steady-state value at ambient temperature within a 15 minute (900 s) time period. Therefore, at the start of each on-cycle the initial temperature used in Eq. (5.1), T_0, is the ambient air temperature (~25 °C). If a shorter period for the off-cycle was to be simulated, then Eq. (5.2) would be required.

5.3.4 External Air Temperature for the Base and Finned Cases

The temperature of the exhaust air for the on-cycle has been determined as the air exits the fuel cell cooling channels. However, this information alone is insufficient for the convection heat transfer relations associated with flow past the metal hydride tanks. As the air flows over the exterior of the tanks, the thermal interaction with the tanks causes a decrease in the temperature of the air since energy is transferred from the air stream into the hydride tanks. An average temperature value is required for the convection heat transfer relations, which is calculated as follows:

$$T_{air}=\frac{T_{in}+T_{out}}{2} \tag{5.3}$$

where T_{in} is calculated from Eq. (5.1) and Eq. (5.2) for the on and off-cycles respectively, and T_{out} represents the temperature after the air stream has interacted with the hydride tanks. T_{out} is calculated by simultaneously solving Eq. (5.3) and the following energy balance, which accounts for the energy transferred to the metal hydride tanks.

$$h_{side} A_{side} \left(T_{air} - T_{side} \right) = m_a c_{pa} \left(T_{in} - T_{out} \right) \tag{5.4}$$

where h_{side} is the convection coefficient along the side wall of the tank, A_{side} is the area of the side wall, T_{side} is the average external temperature of the side wall, m_a is the mass flow rate of the air, and c_{pa} is the specific heat capacity of the air stream.

5.3.5 Air Temperature for the Annular Case

Because the exhaust air flows through a narrow circular duct for the annular case, it experiences a large temperature gradient in the z-direction. A separate subdomain is used to account for the energy transferred to the metal hydride tanks as a function of axial position through the cylinder. Assuming incompressible flow and viscous dissipation is negligible, the equation describing air temperature is as follows:

$$\rho_a c_{pa} A_o \frac{\partial T_{air}}{\partial t} + m_a c_{pa} \frac{\partial T_{air}}{\partial z} = h_{si} P \left(T_{si}(z) - T_{air} \right) \tag{5.5}$$

where ρ_a is the density of the air, A_o is the cross-sectional area of the channel, h_{si} is the convection coefficient along the interior wall, P is the perimeter of the interior channel opening, and T_{si} is the local temperature of the wall at each node along the interior channel of the tank. The inlet value of T_{air}, at z = 0 cm, is calculated from Eq. (5.1) for each on-cycle. During the off-cycle heat transfer through the interior wall is assumed to be negligible; therefore, an expression for the air temperature is not required.

5.3.6 Convection Correlations

The base and finned cases involve a cylinder in cross flow. The average convection coefficient is determined using the correlation due to Hilpert [22]:

$$Nu_D = (0.683) Re_D^{0.466} Pr^{1/3} \tag{5.6}$$

where Pr is the Prandtl number of the air stream, and the Reynolds number, Re_D, is calculated as follows [22]:

$$Re_D = \frac{\rho_a v_m D}{\mu_a} \tag{5.7}$$

where v_m is the mean free stream velocity of the air, D is the diameter of the tank, and μ_a is the dynamic viscosity of the air. This yields a convection coefficient of ~12.5 W m^{-2}K^{-1} for the base case during the on-cycle.

For the off-cycle, there is no forced air stream; therefore the heat transfer is due to natural convection. The average convection coefficient over the entire circumference of the cylinder is determined using the correlation due to Churchill and Chu [22]:

$$Nu_D = \left\{ 0.60 + \frac{0.387 Ra_D^{1/6}}{\left[1 + \left(0.559/Pr\right)^{9/16}\right]^{8/27}} \right\}^2 \tag{5.8}$$

The Rayleigh number, Ra_D, is determined as follows:

$$Ra_D = \frac{g\left(T_s - T_\infty\right) D^3}{T_f \nu \alpha} \tag{5.9}$$

where g is the acceleration due to gravity, T_s is the temperature on the surface of the tank, T_f is the film temperature ($T_f = [T_s + T_\infty]/2$), v is the kinematic viscosity, and α is the thermal diffusivity. Eq. (5.8) and Eq. (5.9) are entered directly into the metal hydride model since the convection coefficient due to natural convection varies as the temperature difference between the tank surface and the ambient air varies. The properties of air for the off-cycle are assumed to be constant at the average film temperature (295 K) and are summarized in Table 5.5.

Table 5.5 - Properties of air during the off-cycle [22].

Parameter	Value
Thermal conductivity, k (W m^{-1}K^{-1})	2.59 x 10^{-3}
Kinematic viscosity, v (m^2 s^{-1})	15.44 x 10^{-6}
Thermal diffusivity, α (m^2 s^{-1})	21.84 x 10^{-6}
Prandtl number, Pr	0.7083

The addition of 50 fins should increase the heat transfer significantly. This increase in heat transfer can be accounted for by using an equivalent convection coefficient. This convection coefficient can then be applied to the original geometry of the model, negating the need to model all of the fins separately. An equivalent convection coefficient can be defined using the following equation for overall efficiency of a finned surface [22]:

$$h_{fin} A_{side} = h_{base} A_t \left[1 - \frac{N A_f}{A_t} \left(1 - \eta_f \right) \right] \tag{5.10}$$

where A_t is the total surface area including fins and base, N is the number of fins, A_f is the surface area of each fin, and η_f is the efficiency of a single fin. The thermal mass of the fins is neglected. The fin efficiency is determined to be 98.5%, which yields an effective convection coefficient of ~170 W m^{-2}K^{-1} during the on-cycle.

For the annular case, the air is flowing through a small circular duct. For fully developed turbulent flow in circular tubes the following correlation can be used [22]:

$$Nu_\infty = \frac{(f/8)\,\mathrm{Re}_D\,\mathrm{Pr}}{1.07 + 12.7(f/8)^{1/2}\left(\mathrm{Pr}^{2/3} - 1\right)} \tag{5.11}$$

where the friction factor, *f*, is calculated by the following equation for a smooth surface [22]:

$$f = 0.184\,\mathrm{Re}_D^{-1/5} \tag{5.12}$$

Since the tube is short, $L/D \approx 32$, it cannot be assumed that the turbulent air flow is fully developed. The convection coefficient for the entry region will exceed the convection coefficient for fully developed flow. To account for the entry effects Eq. (5.11) can be corrected assuming a square-edged entrance as follows [28]:

$$\frac{Nu_m}{Nu_\infty} = 1 + \frac{2.4254}{\left(L/D_o\right)^{0.676}} \tag{5.13}$$

where Nu_m is a mean Nusselt number for the entire length of the tube, D_o is the diameter of the interior opening, and L is the length of the tube. Although Eq. (5.13) yields a mean Nusselt number, it is assumed that this expression can also be used to approximate the local convection coefficient.

6 Results and Discussion

6.1 Grid Independence

Prior to comparing solutions generated by the model, a grid independence test was performed to ensure that an appropriate mesh size was utilized. The test was performed for the finned case and the annular case separately since they use different geometries and different mesh patterns. The base case was not analyzed separately since the mesh is identical to the finned case. The results of this test are given in Figure 6.1 for the finned case and Figure 6.2 for the annular case based on a comparison of the metal hydride density profile at the end of 2.5 hours of operation. The actual mesh patterns and solve times are shown in Figure 6.3 and Figure 6.4.

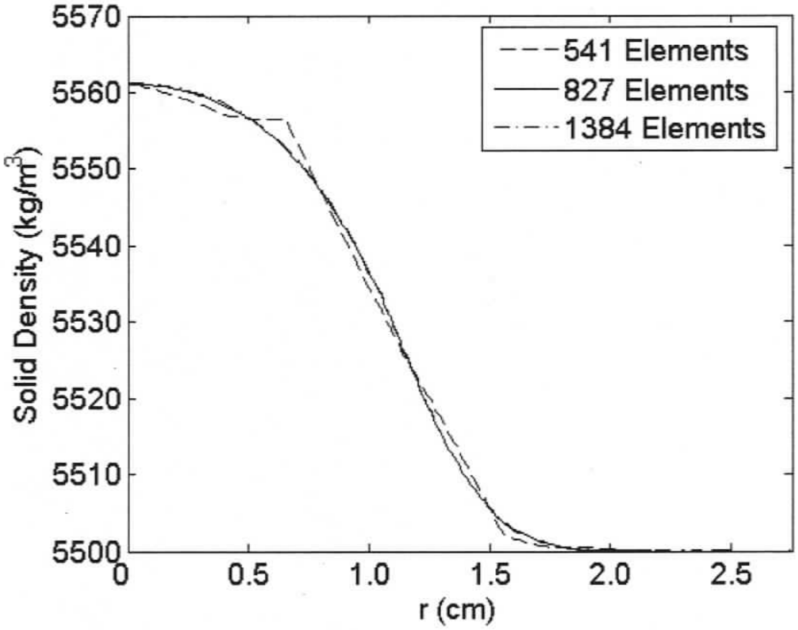

Figure 6.1 – Results of the grid independence test for the finned case displaying the density profile of the metal hydride at *z* = 12.2 cm after 2.5 hours of operation.

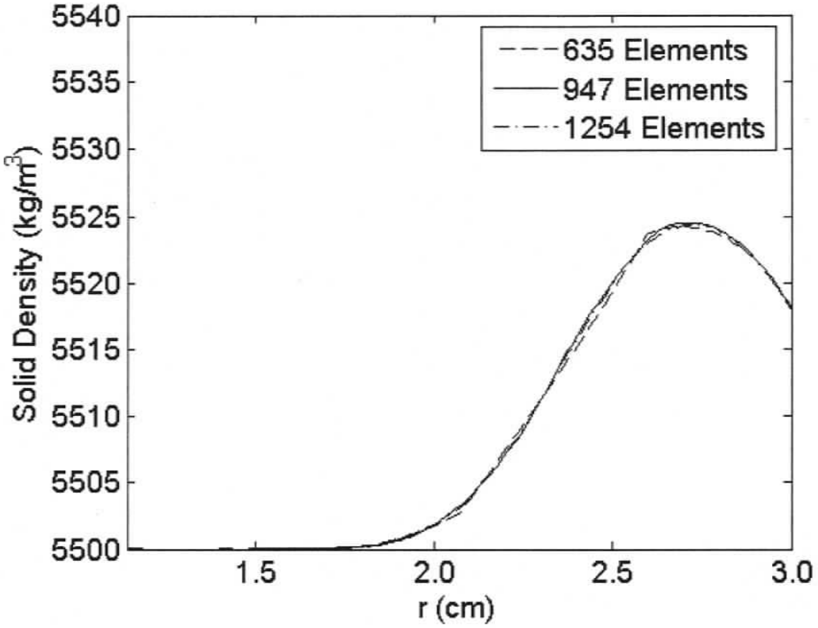

Figure 6.2 – Results of the grid independence test for the annular case displaying the density profile of the metal hydride at z = 12.2 cm after 2.5 hours of operation.

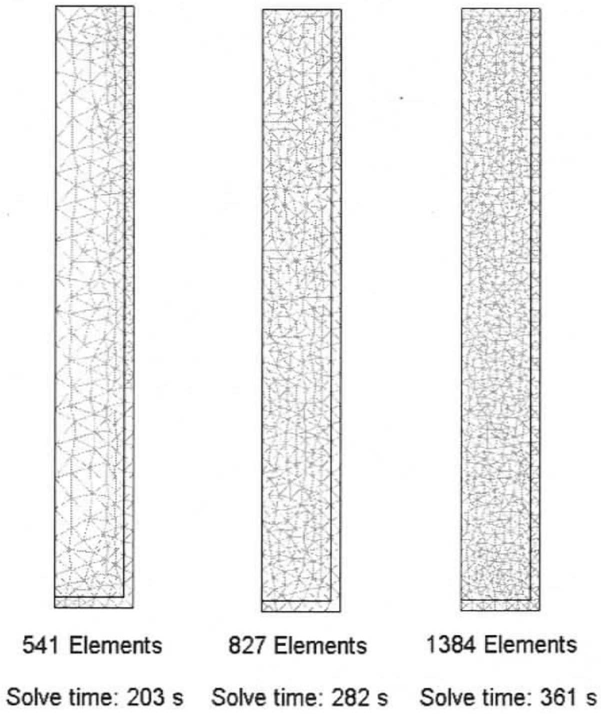

Figure 6.3 – Mesh sizes and solve times generated for the finned case during the grid independence test.

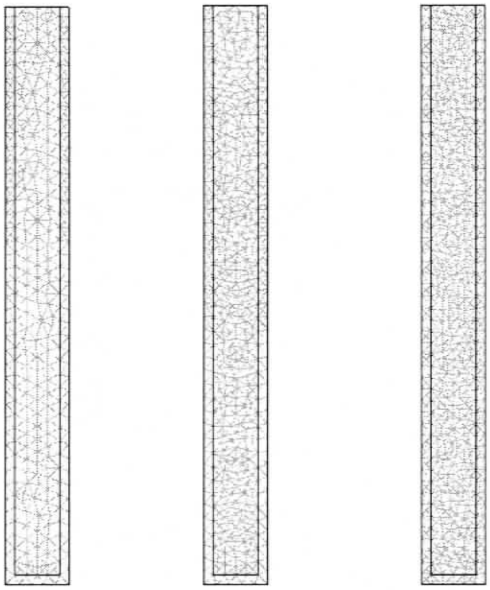

635 Elements · Solve time: 198 s

947 Elements · Solve time: 261 s

1254 Elements · Solve time: 309 s

Figure 6.4 – Mesh sizes and solve times generated for the annular case during the grid independence test.

From Figure 6.1 and Figure 6.2 it can be seen that the different mesh sizes result in slightly different curves. The initialized mesh sizes of 541 for the finned case and 635 for the annular case generate rough curves, therefore refined mesh patterns should be used to produce curves that are smooth. For mesh sizes above 827 elements for the finned case, and above 947 elements for the annular case the result does not significantly change. Therefore these mesh sizes were selected to ensure grid independence while also enabling quick solve times.

6.2 Model Application

As described earlier, the dynamic load profile serviced by the fuel cell system is assumed to be a series of on-off step functions lasting for 2.5 hours, which is 5 full cycles. After the 5 complete cycles approximately 89% of the hydrogen contained in the tank is consumed, as seen in Figure 4.1. All three of the cases are subject to the same hydrogen demand load. The performance of the three storage systems is compared by studying the pressure of the hydrogen gas within the tank throughout the 2.5 hours of pulsed operation. In order to understand the details of the behaviour within a metal hydride tank three additional plots are generated in addition to the pressure plot; the metal hydride density profile throughout the 2.5 hours of operation, the temperature profile during one on-cycle, and a profile of the rate of hydrogen desorption during one on-cycle. Because the base case was only able to provide hydrogen for two complete cycles there is little temporal variation in these parameters, and the plots would provide little useful information. Therefore, the three profile plots are generated to compare the finned and annular cases only.

6.2.1 Hydrogen Pressure Comparison

Figure 6.5 shows the average pressure of the hydrogen within the tank for all three cases. Since there is a minimal pressure gradient throughout the tank, the pressure at the centre of the metal hydride domain is used as the overall average pressure.

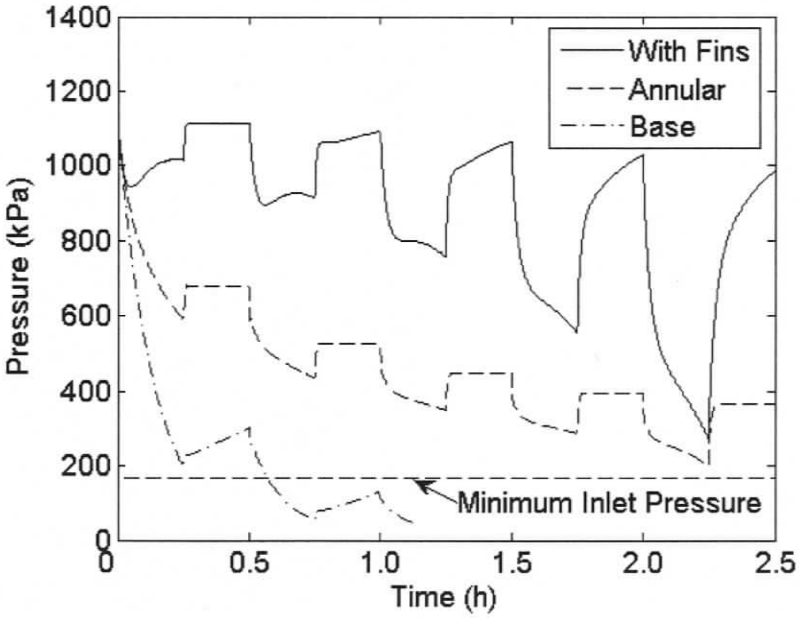

Figure 6.5 – Hydrogen gas pressure inside the metal hydride tank during the 2.5 hours of pulsed operation, showing the comparison between the base, finned, and annular cases. The minimum required inlet pressure to the Nexa^{TM} fuel cell is also shown.

The base case is the original tank with no heat transfer enhancements. Figure 6.5 shows that for the first two cycles the base case is able to provide hydrogen at the required flow rate. However, the pressure within the tank, and therefore the delivery pressure of the hydrogen is significantly lower than the other two cases. The fuel cell requires a minimum hydrogen inlet pressure of 170 kPa (absolute) as shown in Figure 6.5, which the base case cannot maintain during the second on-cycle. During the third on-cycle the base case reaches a pressure of zero, indicating that the dehydriding reaction rate is insufficient to satisfy the demand flow rate although the tank is still ~ 60% full. The reason for the decrease in the minimum pressure for each cycle as the tank empties is due to the progression of the reaction zone towards the centre of the tank, and the increasing thermal resistance due to the increasing distance the thermal energy must travel through the hydride bed. Essentially, the desorption is limited by heat transfer, a well known issue with metal hydride storage systems.

Because the base case is unable to provide the required hydrogen flow, the tank design is modified to enhance the thermal coupling of the fuel cell and the hydrogen storage system. The first modification is the addition of 50 fins along the exterior of the side wall of the tank. Figure 6.5 shows that the finned geometry is able to maintain a pressure that is well above that required by the fuel cell. However, the minimum pressure maintained during the on-cycles drops significantly as the tank empties. During the second cycle the pressure is maintained at a minimum value of 950 kPa, while during the fifth cycle the pressure drops to 275 kPa. As noted in the previous paragraph, this decrease is caused by the increasing resistance of the hydride bed. As the dehydriding reaction proceeds away from the external wall the benefits of using fins are reduced. Pressure values that are too high make for a system that must rely more heavily on relief valves for safety or require a thicker tank wall. Other drawbacks to the finned case are the larger volume occupied by the tank due to the external fins and the additional mass associated with the fins. Figure 4.4 shows the outer diameter that is required for the finned configuration. Metal hydrides are often used for hydrogen storage in scenarios where size is a key design element, because of the advantageous volumetric capacity. However, if a tank with external fins is used, this advantage is diminished since more space is required. This may not be critical when compared to the base case given the fact that an air flow region is required for the base case as well. A design that limits the volume required for exterior air flow while increasing heat transfer would be preferable. A practical concern with the external fin geometry is the frailty of the finned surface which can be easily damaged, unlike a bare cylinder. Also, the mass of the fins increases the total mass of the hydride tank from approximately 2.2 kg to 2.9 kg. This is a significant amount especially considering that metal hydride systems already suffer from high mass compared to other hydrogen storage options. Coupling with the fuel cell may require a complicated design of the exterior ducting as well as making it more difficult to interchange tanks. It has also been assumed that the air flow duct is insulated and that all energy interactions are between the tank and the air, which is a scenario that may not be easy to produce. One advantage to this design is the potential ease in manufacturing such a tank. The cylindrical tank can be formed as usual, and a finned sleeve can be inserted on the tank afterwards.

A second method for heat transfer enhancement is to use an annular tank design, and pipe the exhaust air stream from the fuel cell through the central tube. Figure 6.5 shows that the annular geometry is able to provide the hydrogen flow rate while maintaining a pressure above the minimum requirement of the fuel cell. The peak pressures in this case are less than the finned configuration, and the variability is also reduced. The minimum pressure maintained during the first cycle is 590 kPa, while the minimum pressure during the fifth on-cycle is 200 kPa. This is an improvement over the 71% reduction experienced for the finned case and is due to the reduced distance the thermal energy must pass through for the annular tank. This shorter radial distance through the hydride bed is illustrated well by Figure 4.4. Other advantages of the annular design are the reduced volume and mass, as compared to the finned geometry, and a more robust structure. This configuration also requires a simpler ducting system through the interior tube that would facilitate replacement of the tanks for refuelling. The ducting system for this configuration also ensures that the air stream is isolated from the surroundings and maximum energy exchange is facilitated. One drawback to this design is the possible complexity of manufacturing an annular tank. However, depending on the manufacturing techniques that are employed this may or may not be a more complicated process than the finned tank. Another drawback is the potential for a pressure drop as the air flows through the narrow interior tube that may be too high for the fuel cell exhaust fan. An additional fan may be required to assist with the air flow.

6.2.2 Metal Hydride Density Profile

Figure 6.6 and Figure 6.7 show the density profile of the metal hydride solid at cross section z = 12.2 cm throughout the 2.5 hours of operation for the finned and annular cases respectively. The reason for the decrease in metal hydride density as time proceeds is due to the decreasing amount of hydrogen that is part of the solid structure as it is desorbed and released in gaseous form. This is based upon the governing equation regarding the solid mass balance which is Eq. (3.4). So Figure 6.6 and Figure 6.7 are an indication of the varying hydrogen concentration in the metal hydride bed and therefore the state of fill of the tank throughout the 2.5 hours of operation. These profile plots illustrate the different desorption patterns in the finned and annular configurations and specifically display the locations in the tank where desorption takes place as time proceeds.

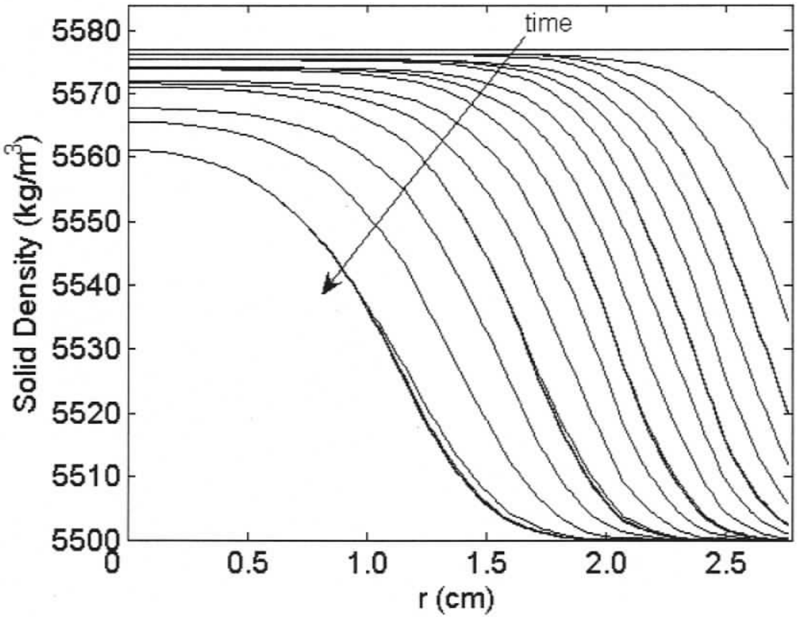

Figure 6.6 – Density profiles of the metal hydride solid for the finned case at cross section *z* = 12.2 cm for all times (*t* = 0 – 2.5 h).

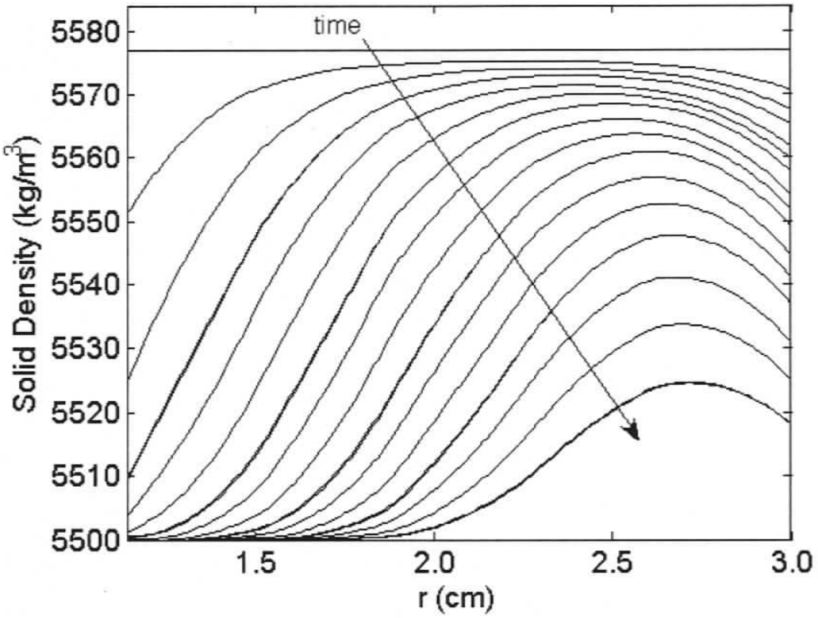

Figure 6.7 – Density profiles of the metal hydride solid for the annular case at cross section z = 12.2 cm for all times (t = 0 – 2.5 h).

As described above in Chapter 2, Figure 6.6 shows that the hydrogen is desorbed in a wave-like manner beginning at the exterior wall, where the heat is provided, and proceeds towards the centre of the tank. This accounts for the majority of the gas desorbed. A secondary desorption is also occurring uniformly throughout the tank during certain time intervals. Along the left edge of Figure 6.6, at r = 0 cm, it can be seen that as time progresses the density at this point decreases. This indicates that a small amount of hydrogen is being desorbed from the centre of the tank, and not just near the edge. Because of the pulsed square-wave nature of the hydrogen demand, there are short periods where desorption is occurring nearly uniformly throughout the bed where the alloy is not locally depleted. When the hydrogen demand is switched on, the hydrogen gas that has built-up within the tank exits and the pressure drops, creating a low enough pressure within the tank to initiate the desorption reaction throughout the regions in the tank that still contain hydrogen. This more uniform reaction exists momentarily until it is restricted by heat transfer limitations (i.e. the temperature decreases locally, causing the equilibrium pressure, which is temperature dependent, to drop). For the remainder of a period, the reaction dominates in locations where the thermal wave reaches the reaction zone.

Figure 6.7 shows a different desorption pattern to that of Figure 6.6 due to the annular tank design. In this case the heat is supplied at the centre of the tank, so one would expect the desorption to proceed in a wave-like manner from the centre of the tank to the exterior wall. However, this is not exactly what is observed in Figure 6.7, since there is a significant amount of desorption occurring adjacent to the exterior wall, which is insulated. Due to the high conductivity of the aluminum tank wall, the heat provided at the centre of the tank is able to travel through the bottom of the tank and make its way up the side wall. Therefore, there is an effective heat source along the side wall due to the aluminum, and some desorption occurs here. This indicates that the annular configuration not only benefits from some additional effective heat sources along the exterior of the metal hydride bed due to the aluminum tank walls. This phenomenon also illustrates the importance of including the aluminum tank wall when modelling different metal hydride tank configurations.

6.2.3 Temperature Profile

Figure 6.8 and Figure 6.9 show the temperature profile of the metal hydride solid at cross section z = 12.2 cm for one on-cycle at times t = 1.5 – 1.75 h for the finned and annular cases respectively. The temperature within the tank during cycling is not as uniform as the pressure. It can be seen from Figure 6.8 and Figure 6.9 that a bulk average temperature value would have little meaning. Since the heat transfer equations are active in the tank walls these profile plots include the temperatures in the aluminum walls.

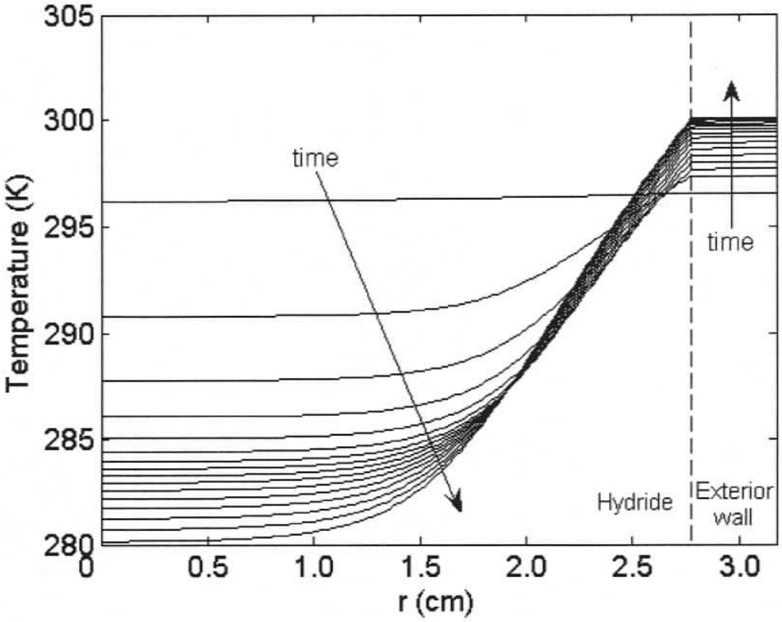

Figure 6.8 – Temperature profiles for the finned case at cross section z = 12.2 cm for one discharge period at times t = 1.5 – 1.75 h.

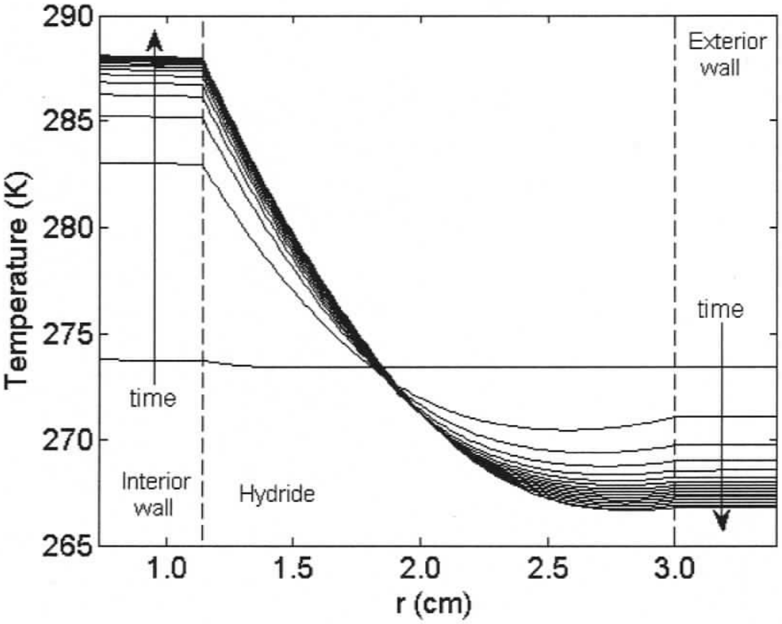

Figure 6.9 – Temperature profiles for the annular case at cross section z = 12.2 cm for one discharge period at times t = 1.5 – 1.75 h.

Figure 6.8 further illustrates the wave-like desorption pattern discussed above in Section 6.2.2 for the metal hydride density profile. Heat is provided at the right hand side of

Figure 6.8, and due to the high conductivity of the aluminum tank wall, the temperature profile is relatively flat in this region. Due to the poor conductivity of the metal hydride bed the temperature profile drops, until the heat reaches the reaction zone. This is located at approximately r = 1.6 cm during this cycle, and it can be seen that the energy is not able to pass the reaction zone since the endothermic desorption reaction consumes it; therefore the temperature profile is flat from the reaction zone to the centre of the tank. The temperature along the external wall, at r = 3.175 cm, is actually increasing throughout the on-cycle. This is due to the increased heat transfer rate because of the fins. Without any enhancements this temperature would drop and thermal energy would not reach the reaction zone as fast, thus causing a greater pressure drop as observed in Figure 6.5.

Figure 6.9 confirms the behaviour described in Section 6.2.2 for the metal hydride density profile. In this configuration the heat is provided along the centre wall of the tank at r = 0.74 cm. The temperature profile is very similar to that observed for the finned case except that the direction has changed since heat is introduced from the centre and not the exterior wall. The main difference between these two cases is the heat provided by the aluminum wall, seen at r = 3.0 – 3.4 cm in Figure 6.9. Heat energy provided by the side wall can be seen by a small increase in temperature of the metal hydride bed in the alloy adjacent to the wall at this location (z = 12.2 cm). At z locations closer to the base, the impact of heat conduction through the wall is greater. Another difference is that the temperature at the beginning of an on-cycle is level at 298.15 K for the finned case and only ~273.5 K for the annular case. This is because the tank in the finned case is exposed to ambient air during the 15 minute off-cycle whereas the annular tank is assumed insulated; therefore the finned tank levels off at ambient temperature and the annular tank levels off at a temperature based on a redistribution of the temperature of the system when the off-cycle begins. Because the annular tank begins the on-cycle at a lower temperature, the temperature throughout the demand cycle remains lower than that of the finned tank. This is one reason why the pressures observed for the finned tank are higher than the annular tank. Higher temperatures enable higher pressures, since the equilibrium desorption pressure increases with temperature. These results suggest that allowing thermal interactions with environmental air on the outside wall of the annular tank should increase performance. Thus, the assumption of an insulated outer boundary is a conservative constraint.

6.2.4 Hydrogen Desorption Profile

Figure 6.10 and Figure 6.11 illustrate the location along the r-axis where desorption is occurring at cross section *z* = 12.2 cm, for the hydrogen discharge period at times *t* = 1.5 h – 1.75 h. The y-axis is labelled as hydrogen absorption because the overall *m* term is configured to be positive for absorption and negative for desorption. Therefore, although the y-axis is labelled as absorption, the values in the plot are negative, indicating that desorption is occurring.

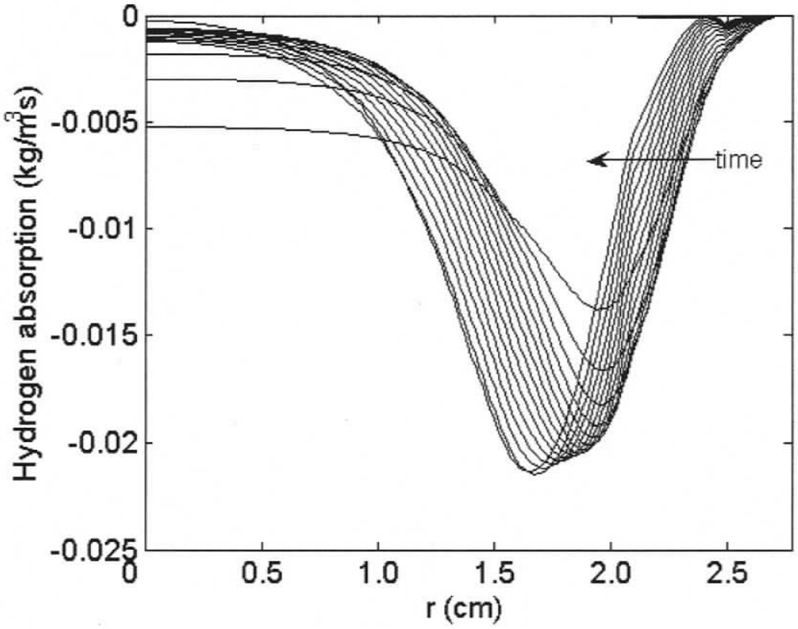

Figure 6.10 – Profiles of the rate of hydrogen mass being desorbed from the metal hydride bed for the finned case at cross section *z* = 12.2 cm for one discharge period at times *t* = 1.5 – 1.75 h.

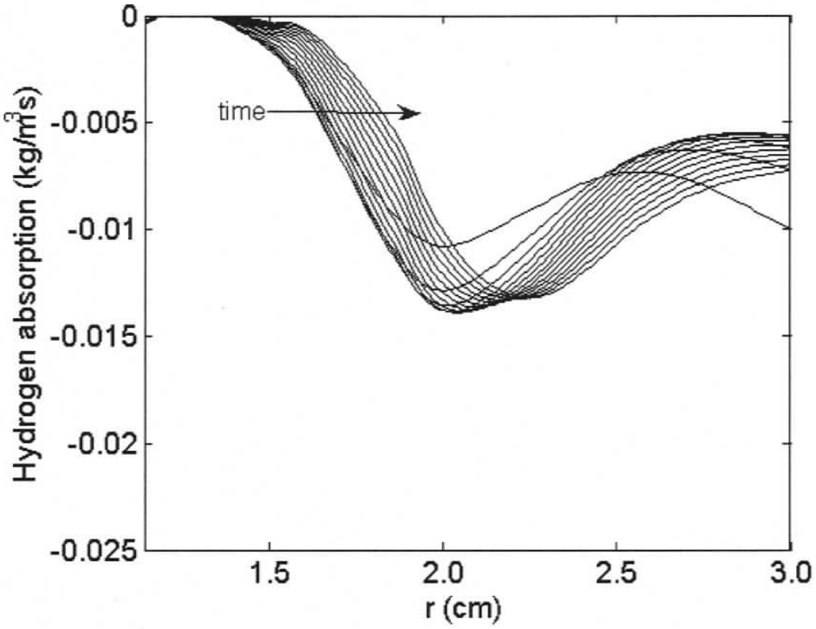

Figure 6.11 – Profiles of the rate of hydrogen mass being desorbed from the metal hydride bed for the annular case at cross section *z* = 12.2 cm for one discharge period at times *t* = 1.5 – 1.75 h.

Figure 6.10 shows a lower minimum point for desorption than Figure 6.11. The dip in the curves represents the location of the main reaction zone. The finned case therefore has a more concentrated reaction zone due to the higher temperatures and single heat source (only external wall) as described above in Sections 6.2.2 and 6.2.3. Figure 6.11 shows that the annular case does not reach the same magnitude of desorption in any single location as the finned case; however it has a desorption pattern that is more spread out across the radius of the tank. This is due to the additional effective heat source provided by the conductance of heat through the aluminum tank walls that allows desorption to occur within the hydride bed adjacent to the exterior wall at *r* = 3.0 cm.

The metal hydride density, temperature, and hydrogen desorption profiles shed some light into the behaviour of metal hydride tank configurations that are subjected to a pulsed hydrogen demand load. These results reveal complex temperature and pressure behaviour that may enable creative solutions to the heat transfer problem.

7 Conclusions

This chapter will summarize the major findings in this thesis and discuss recommendations for future work. It begins with a summary of the objectives laid out in Chapter 1 in order to place the conclusions in context. The objectives of this thesis are the following three points:

- develop a comprehensive, two-dimensional, numerical model describing the behaviour in a metal hydride hydrogen storage tank;
- develop heat transfer relations that enable the metal hydride model to be coupled with a fuel cell system;
- examine the effects of heat transfer enhancements and storage tank configurations on a thermally coupled metal hydride hydrogen storage and fuel cell system.

7.1 Conclusions

This thesis describes the development of a comprehensive two-dimensional mathematical model of a metal hydride hydrogen storage tank. The model includes heat and mass transfer, as well as reaction kinetics. Both absorption and desorption are included in the model simultaneously so that any manner of cyclic loading can be investigated. The phenomenon of hysteresis is also included in the model by utilizing two different expressions for the absorption and desorption equilibrium pressures. The model has also been validated against a well known experimentally validated model. The model has been implemented in a program called COMSOL Multiphysics^{TM} which utilizes the finite element method to solve the governing equations. Since this validated model is robust and has quick solve times, it can be utilized to study the behaviour of metal hydride tanks and lead to better system designs while reducing the amount of time-consuming experiments required.

Metal hydride hydrogen storage systems are usually used in conjunction with fuel cell systems. PEM fuel cell systems usually have a waste exhaust stream due to the operation of the system at temperatures above ambient. Since the desorption reaction in metal hydride tanks is endothermic there is the potential to utilize the waste heat from the fuel cell to enhance the desorption of the hydrogen gas in the metal hydride tank. This thesis describes the development of a series of heat transfer relations that effectively couple the metal hydride model to a fuel cell system by replicating the thermal conditions experienced on the tank walls in a coupled scenario. These relations encompass the temperature of the exhaust air stream flowing past the tank and convection correlations that are based upon information provided by Ballard® and data acquired from experimental testing of the Nexa™ fuel cell module. The relations were developed for the base and finned cases and the annular case since the different geometry of the two setups creates two unique scenarios. These relations were implemented in the model by applying them as boundary conditions. With the thermal coupling of a PEM fuel cell to metal hydride hydrogen storage tanks complete, the model was used to examine the effectiveness of heat transfer enhancements.

Thermal coupling of a metal hydride storage system and a fuel cell module was investigated for a specified time-dependent electrical demand. The ability of three different metal hydride tanks to satisfy the minimum hydrogen delivery pressures were simulated and compared. For the dynamic cycle used in this study, the base case (bare cylinder) is unable to service the required flow of hydrogen gas. A tank with 50 external fins meets the required demand however the peak pressure is considerably higher than what is necessary. Furthermore, this configuration satisfies fuel flow requirements but occupies more volume and has a higher mass, which may partially diminish the advantage of using a metal hydride system. The fins are also frail and may be subject to damage. An annular tank design was found to provide hydrogen gas at the required flow rate and pressure stipulated by the fuel cell. The peak pressures in this case are lower than with the finned tank, making the system somewhat safer. The annular tank design requires less volume than a finned design and may be easier to integrate to the fuel cell. The annular configuration also provides a robust design, and a simple ducting system that reduces energy lost to the surroundings. It was found that although the exterior wall in the annular case is assumed insulated, heat conduction through the aluminum from the inner wall to the outer wall helps maintain pressure throughout the operating period.

7.2 Recommendations

The following points are either projects planned for the future that were deemed to be beyond the scope of this thesis, or suggestions for future researchers who plan to take on the challenge of metal hydride hydrogen storage systems:

- A test apparatus has been built for detailed and thorough testing of metal hydride tanks so that the mathematical model can be experimentally validated directly without relying on tests performed by other researchers on other alloys. This will add even more credibility to the results generated by the model;

- The advection and heat transport by convection terms were not included in the energy equation. It would be valuable to perform a study on the validity of these exclusions that involves extensive experimental comparison;

- There are a number of heat transfer enhancing designs for metal hydride tanks that would benefit from optimization work. One example is the optimization of the spacing, size, and number of fins used on a finned tank to optimize heat transfer, another is the optimization of the size of the central opening for an annular tank to increase heat transfer without restricting fluid flow, and one final optimization project could be to analyze the potential of using a solid tank with a hollow core region, the size and materials used to create the hollow core could be optimized;

- This thesis revealed some interesting dynamic behaviour for the temperature and desorption rates inside a metal hydride tank. A more detailed investigation into this behaviour could lead to some creative solutions to the heat transfer problem associated with metal hydride storage systems;

- A potential avenue for fuel cells that has emerged in the last few years is to replace batteries particularly in small-scale electronic devices such as cell phones, PDAs, and laptops. The higher power density and quicker "recharge" times associated with fuel cell systems could make this field an ideal starting market to showcase the advantages of the technology and facilitate the use of fuel cells in other areas. Due to the small size requirements in this area, metal hydride storage tanks seem to be the ideal hydrogen storage media, and therefore there is the need for small metal hydride "cartridges" to be designed for use in these systems. The mathematical model developed in this thesis could be used to facilitate this design process and generate some innovative solutions.

References

1. Honda Motor Co. Hydrogen Tank – The Honda FCX. [Online document – cited February 2, 2006]. Available http: http://world.honda.com/FuelCell/FCX/tank/

2. Schlapbach L, and Züttel A. Hydrogen-storage materials for mobile applications. Nature 2001;414:353-358.

3. Honda Motor Co. Tokyo 2005 – Tokyo Motor Show. [Online document – cited February 2, 2006]. Available http: http://world.honda.com/Tokyo2005/fcx/index02.html

4. Sandrock G. A panoramic overview of hydrogen storage alloys from a gas reaction point of view. Journal of Alloys and Compounds 1999;293-295:877-888.

5. Mayer U, Groll M, and Supper W. Heat and mass transfer in metal hydride reaction beds: experimental and theoretical results. Journal of the Less-Common Metals 1987;131:235-244.

6. Supper W, Groll M, and Mayer U. Reaction kinetics in metal hydride reaction beds with improved heat and mass transfer. Journal of the Less-Common Metals 1984;104:279-286.

7. Sun DW, and Deng SJ. Study of the meat and mass transfer characteristics of metal hydride beds. Journal of the Less-Common Metals 1988;141:37-43.

8. Sun DW, and Deng SJ. Study of the heat and mass transfer characteristics of metal hydride beds: a two-dimensional model. Journal of the Less-Common Metals 1989;155:271-279.

9. Sun DW, and Deng SJ. Numerical solution of the two-dimensional non-steady heat and mass transfer problem in metal hydride beds. International Journal of Hydrogen Energy 1990;15:807-816.

10. Sun DW. Designs of metal hydride reactors. International Journal of Hydrogen Energy 1992;17:945-949.

11. Ram Gopal M, and Murthy SS. Prediction of heat and mass transfer in annular cylindrical metal hydride beds. International Journal of Hydrogen Energy 1992;17:795-805.

12. Ram Gopal M, and Murthy SS. Parametric studies on heat and mass transfer in metal hydride beds. Chemical Engineering and Processing 1993;32:217-223.

13. Jemni A, and Ben Nasrallah S. Study of two-dimensional heat and mass transfer during absorption in a metal-hydrogen reactor. International Journal of Hydrogen Energy 1995;20:43-52.

14. Jemni A, and Ben Nasrallah S. Study of two-dimensional heat and mass transfer during desorption in a metal-hydrogen reactor. International Journal of Hydrogen Energy 1995;20:881-891.

15. Ben Nasrallah S, and Jemni A. Heat and mass transfer models in metal-hydrogen reactor. International Journal of Hydrogen Energy 1997;22:67-76.

16. Jemni A, Ben Nasrallah S, and Lamloumi J. Experimental and theoretical study of a metal-hydrogen reactor. International Journal of Hydrogen Energy 1999;24:631-644.

17. Mat M, and Kaplan Y. Numerical study of hydrogen absorption in an $Lm - Ni_5$ hydride reactor. International Journal of Hydrogen Energy 2001;26:957-963.

18. Demircan A, Demiralp M, Kaplan Y, Mat MD, Veziroglu TN. Experimental and theoretical analysis of hydrogen absorption in $LaNi_5$-H_2 reactors. International Journal of Hydrogen Energy 2005;30:1437-1446.

19. Nakagawa T, Inomata A, Aoki H, Miura T. Numerical analysis of heat and mass transfer characteristics in the metal hydride bed. International Journal of Hydrogen Energy 2000;25:339-350.

20. Inomata A, Aoki H, Miura T. Measurement and modelling of hydriding and dehydriding kinetics. Journal of Alloys and Compounds 1998;278:103-109.

21. Jiang Z, Dougal RA, Liu S, Gadre SA, Ebner AD, Ritter JA. Simulation of a thermally coupled metal-hydride hydrogen storage and fuel cell system. Journal of Power Sources 2005;142:92-102.

22. Incropera FP and DeWitt DP. Fundamentals of Heat and Mass Transfer. New York: John Wiley & Sons Inc, 2002.

23. Suda S, Kobayashi N, Yoshida K. Reaction kinetics of metal hydrides and their mixtures. Journal of the Less-Common Metals 1980;73:119-126.

24. White FM. Fluid Mechanics, 4th Edition. New York: Mc-Graw Hill, 1999

25. Sandrock G, Thomas G. IEA/DOE/SNL Hydride Databases [Online database – cited February 17, 2006]. Available http: http://hydpark.ca.sandia.gov

26. BALLARD® Nexa™ Power Module User's Manual (MAN5100078). Ballard Power Systems Inc., 2003.

27. Ovonic® Solid Hydrogen Storage System Portable Canisters Brochure. Ovonic Hydrogen Systems LLC, 2005.

28. Bhatti MS, Shah RK, in: Kakaç S, Shah RK, Aung W (Eds.), Handbook of Single-Phase Convective Heat Transfer, John Wiley & Sons, New York, 1987, pp. 4.1-4.166.